Title Page

Acute adenoviral cardiac infection elicits an arrhythmogenic substrate prior to inflammatory myocardial remodeling and myocarditis

Rachel L. Padget[1,2,3], Grace A. Blair[1,2,3], Michael D. North[4], Michael J. Zeitz[2,3], Mira T. Tanenbaum[4], D. Ryan King[1,2,3], Gregory S. Hoeker[2,3], Sharon A. Swanger[2,4,5], Steven Poelzing[2,3,4,6], James W. Smyth[2,3,4,6,7]

[1] Graduate Program in Translational Biology, Medicine, and Health, Virginia Tech, Blacksburg, VA 24061, USA
[2] Fralin Biomedical Research Institute at Virginia Tech Carilion, Roanoke, VA 24016, USA
[3] Center for Vascular and Heart Research, FBRI at VTC, Roanoke, VA 24016, USA
[4] Virginia Tech Carilion School of Medicine, Roanoke, VA 24016, USA
[5] Department of Biomedical Sciences and Pathobiology, Virginia-Maryland College of Veterinary Medicine, Virginia Tech, Blacksburg, VA 24061, USA
[6] Department of Biomedical Engineering and Mechanics, College of Engineering, Virginia Tech, Blacksburg, VA 24061, USA
[7] Department of Biological Sciences, Virginia Tech, Blacksburg, VA 24061, USA

Corresponding author:
James W. Smyth,
Fralin Biomedical Research Institute at VTC,
2 Riverside Circle,
Roanoke,
VA 24016.

Email: smythj@vtc.vt.edu

Total word count: 8526

Abstract

Viral cardiac infection represents a significant clinical challenge encompassing several etiological agents, disease stages, complex presentation, and a substantial lack of mechanistic understanding. Myocarditis is a leading cause of sudden cardiac death in young adults, for which viral infection is the most common cause. Current knowledge in the field is dominated by later phases of disease, and the role of host immune responses in pathogenesis. However, little is known regarding how viral infection can acutely induce an arrhythmogenic substrate in the heart, and how this may create an already dangerous substrate prior to the immune response. Viruses are known to alter gap junction intercellular communication in various cell types, leading us to investigate the impact of infection on cardiomyocyte coupling and electrophysiology. Adenovirus is a leading cause of myocarditis, but due to species-specificity, models of infection are lacking and it is not understood how adenoviruses cause sudden cardiac arrest. Mouse Adenovirus Type-3 (MAdV-3) was recently isolated and reported to be cardiotropic, yet has not been utilized to understand mechanisms of cardiac infection and pathology in the research setting. We have developed MAdV-3 infection as a model to investigate acute cardiac infection and molecular alterations to the infected heart prior to an appreciable immune response or gross cardiomyopathy. By optical mapping we find decreases in conduction velocity concomitant with increased phosphorylation of $Cx43^{Ser368}$, a residue known to regulate gap junction channel function. Additional to changes in gap junctions, patch clamping of MAdV-3-infected adult mouse ventricular cardiomyocytes reveals prolonged action potential duration as a result of decreased I_{K1} and I_{Ks} current density. Turning to human systems, we find that human adenovirus type-5 (HAdV-5) increases phosphorylation of $Cx43^{Ser368}$ and disrupts calcium transients synchrony in human induced pluripotent stem cell-derived cardiomyocytes (iPSC-CMs), indicating common mechanisms with our mouse whole heart and adult cardiomyocyte data. Together, these findings demonstrate that adenoviral infection creates an arrhythmogenic substrate through direct targeting of gap junction and ion channel function in the heart. Such alterations are known to precipitate arrhythmias and likely contribute to sudden cardiac death in acutely infected patients, while preceding the pathological remodeling of subsequent myocarditis disease progression.

Introduction

Viral infection of the heart results in significant morbidity and mortality, representing a major cause of sudden cardiac death (SCD) in young adults where up to a 42% causative incidence of viral-associated myocarditis is reported[1-3]. Viral myocarditis is classified into distinct phases of disease, encompassing an acute phase of active infection where direct viral-mediated damage to myocardial cells occurs and may subsequently progress to a chronic disease phase involving the host immune response[4]. Chronic viral myocarditis can then advance to dilated cardiomyopathy (DCM) and heart failure (HF), with limited clinical options available bar the supportive care and potential need for transplant shared with other forms of end-stage cardiac disease[5,6]. Clinical myocarditis data are understandably dominated by chronic disease, where host immune responses to the initial infection are understood to precipitate pathological remodeling to HF[7]. The molecular mechanisms of acute cardiac infection, and specifically how active viral replication in the myocardium precipitates arrhythmia prior to an appreciable immune response, are not well understood. Indeed, individuals with such direct active cardiac involvement often do not survive the sudden cardiac arrest event triggered by infection and/or do not present with altered cardiac remodeling and function by echocardiography, for example[8,9]. A better understanding of how acute viral infection alters cardiac electrophysiology and function prior to immune infiltration is key in the development of interventions against arrhythmogenesis, in addition to identifying pathways underlying progression to chronic viral myocarditis for therapeutic targeting and/or early diagnosis.

Arrhythmias are the leading cause of sudden cardiac arrest in children and young adults[3,10,11]. Normal cardiac electrophysiological function is achieved primarily through two major components: ion channels localized to specific nanodomains of the sarcolemma, and cell-to-cell electrical coupling at the intercalated disc (ID)[12-14]. The proteins comprising the major cardiac ion channels responsible for generation of the action potential (AP), including $Ca_V1.2$, $Na_V1.5$, Kir2.1, $K_V7.1$, and $K_V11.1$, are subject to dynamic regulation affecting their localization and function. Pathological alterations to the AP, such as prolonged duration due to perturbed channel function, can lead to lethal arrythmias[15]. IDs encompass fascia adherens, gap junctions, the perinexus, desmosomes, and an enrichment of several ion channels to effect mechanical and electrical coupling between adjacent cardiomyocytes[16-21]. Subcellular remodeling of such ID-resident structures and channels is well described as underlying arrhythmogenesis across a breadth of cardiac disease states, including viral infection[22-27].

A rapid and modifiable mechanism of regulating structures at the ID is dynamic phosphorylation of target proteins. A common outcome of increased phosphorylation of gap junctions and ion channels is a positive or negative effect on function[28-30]. In addition to direct impacts, indirect consequences include regulation of ion channel density. For example, increased phosphorylation by PKC on KCNE1 can impair trafficking of the KCNQ1/KCNE1 complex forming the ion channel, $K_V7.1$, and therefore reduce I_{Ks}[31,32]. Changes to gap junction intracellular communication (GJIC) are established in underlying arrhythmias and SCD[33]. Twenty-one human connexins have been identified, with connexin43 (Cx43) being the most ubiquitously expressed throughout the body while also being the primary connexin of the ventricular working myocardium[34]. In addition to electrical coupling, gap junctions play a critical role in propagation of innate and adaptive antiviral immune responses, providing justification for pathogens to target such structures[35-37]. Indeed, we have previously reported Cx43 is specifically down regulated at the transcriptional level and functionally targeted through altered phosphorylation during adenoviral infection in human epithelial cells and induced pluripotent stem cell-derived cardiomyocytes (HiPSC-CMs)[38].

The most common viral families identified as causative agents in SCD and development of viral myocarditis include adenoviruses, coronaviruses (SARS-CoV-2), enteroviruses (Coxsackievirus B3, CVB3), herpesviruses, and parvoviruses, with enteroviruses representing the most intensely researched[10,39,40]. CVB3 is a non-linear, positive-sense single-stranded RNA (ssRNA) virus from the picornavirus family commonly associated with childhood illness and a significant causative agent of viral myocarditis in all ages[41]. The ability of CVB3 to viably infect and replicate across species has resulted in its development as a valuable, and arguably leading, research model for viral myocarditis[27,42,43]. Indeed, the majority of viral myocarditis research has been conducted using CVB3 with an emphasis on the chronic phase of disease[7]. Other viruses known to cause myocarditis, such as adenoviruses, have starkly different biology to CVB3, perhaps most obviously though their double stranded DNA (dsDNA) genomes requiring the virus to colonize the cellular nucleus and uncouple cell cycle regulation for a significantly longer life cycle than a positive-sense RNA virus[41,44,45]. Such differences likely elicit virus-specific pathologies during the acute stage of viral myocarditis, illustrating the need to investigate virus family-specific disease progress and pathology beyond CVB3.

Adenoviruses are non-enveloped, dsDNA viruses, and include over 50 serotypes (now 'types') capable of human infection where they cause a range of illnesses from mild respiratory disease to more severe and potentially fatal conditions such as myocarditis[46]. Tissue tropism is classically attributed to type-specific host cell receptor binding and/or permissiveness of specific cell types to adenoviral replication[47]. Human adenovirus types 2 and 5 (HAdV-2 and -5) are the most predominant causes of adenoviral myocarditis, although additional types are increasingly reported[48-50]. Early adenoviral proteins mimic growth factor signaling and induce cell cycle entry to take advantage of DNA synthesis machinery and replicate viral genomes[45,51,52]. These same signaling pathways target GJIC, as we have previously demonstrated, and likely also impact the cardiac ion channels that shape the AP[28,31,38,53]. Unlike CVB3 however, many HAdVs cannot replicate effectively in mice, resulting in a dearth of understanding regarding adenoviral cardiotropism and virus-specific effects on the heart due to this stringent adenoviral species-specificity[46,54]. Mouse adenovirus type 1 (MAdV-1) has historically been employed in modeling respiratory disease and encephalitis, and while not a 'cardiotropic' virus, additional studies have successfully modeled adenoviral myocarditis in mice using MAdV-1, with an emphasis on inflammation[55-58]. In 2008, mouse adenovirus type-3 (MAdV-3) was isolated as distinct from the previously described MAdV-1 and MAdV-2, and reported to be cardiotropic[59,60]. Development of MAdV-3 as a model for myocarditis, or use of this virus in investigation mechanisms of arrhythmogenesis during acute cardiac infection has been limited, however.

In this study, we successfully employ MAdV-3 to model acute viral cardiac infection in adult mice and confirm similar targeting of Cx43 to that which we previously observed with human adenovirus[38]. Prior to appreciable immune cell infiltration or development of any gross cardiomyopathy, we find slowed conduction velocity concomitant with prolonged AP duration (APD) in infected hearts; two pro-arrhythmogenic phenotypes. Turning to studies in isolated primary adult cardiomyocytes we identify perturbation of I_{KS} and I_{K1} underlies prolonged APD during adenoviral infection. MAdV-3 infection therefore represents a viable and relevant model of acute myocarditis, and targets cardiac conduction through the same mechanisms we have previously found in cell-based human adenovirus studies. Our data demonstrate that acutely infected hearts harbor dangerous and arrhythmogenic alterations at the molecular level and reveal, for the first time, how adenoviral infection can cause SCD prior to cardiomyopathy and development of inflammatory myocarditis.

Materials and Methods

Animals

All animal husbandry and experimental protocols described utilized 8-12 week old C57BL/6J male and female mice, were carried out under NIH guidelines, and approved by the Virginia Tech Institutional Animal Care and Use Committee.

Cell culture

Normal murine mammary gland (NMuMG), A549, (ATCC), 3T6, 293A, and 293FT (Thermo Fisher) were maintained in Dulbecco's Modified Eagle Medium, high glucose with L-glutamine and sodium pyruvate (Genesee Scientific) supplemented with 10% FBS, non-essential amino acids (Gibco) and Mycozap Plus-CL (Lonza).

HiPSC-CM differentiation, expansion, and maturation

HiPSCs (Cell Applications) were differentiated into cardiomyocytes as previously described[61], with modifications. Briefly, iPSCs were seeded in E8 medium (Thermo Fisher) into matrigel (Corning) coated (1:99) 12-well plates with daily media changes for 3 days. Following this, on day 0, medium was changed to CDM3, as defined in[62] with 3 μM CHIR-99021 (Selleckchem) in RPMI for 2 days. On day 2, medium was changed to CDM3 with 2 μM Wnt-C59 (Cayman). On day 4, medium was replaced with CDM3. On day 6, medium was changed to RPMI1640 + B27 (Thermo Fisher) (- insulin) and refreshed on day 8. On day 10, medium was changed to RPMI1640 without glucose + B27. On day 12, cardiomyocytes were expanded as in[63]. Cells were lifted with TrypLE Select Enzyme 10X (Thermo Fisher), washed with PBS 20% FBS and centrifuged at 200 x *g* for 4 min, resuspended in RPMI 1640 + B27 1X with 10% Knock Out Serum Replacement (Gibco) and Thiazovivin 1.0 μM (Selleckchem), and transferred into 10 cm dishes. 24 h later medium was replaced with RPMI 1640 + B27 1X supplemented with 2 μM CHIR-99021 (Selleckchem). Cells were further expanded for 4 passages prior to cryopreservation. IPSC-CMs were verified by the presence of cardiac troponin-T, N-cadherin, and spontaneous contraction under phase microscopy. Prior to experiments, IPSC-CMs were matured in a defined maturation medium composed of oxidative substrates and low glucose for 3 weeks with media changes every 3 days, as previously reported[64].

Virus propagation and titering

MAdV-3 (a generous gift from D. H. Krüger, M.D., Ph.D., Institute of Med. Virology, University Hospital Charité, Berlin) was propagated in NMuMG cells. MAdV-3 was purified by PEGylation and CsCl ultracentrifugation as previously described, and titer was determined by immunofluorescence confocal microscopy in 3T6 cells (Thermo Fisher)[38,65]. HAd5 (ATCC) was propagated in A549 cells and AdlacZ was generated according to manufacturer's instructions from pAd/CMV/V5-GW/LacZ (Thermo Fisher) for purification by CsCl ultracentrifugation and titering in 293A cells as previously described[38,65].

Adult mouse cardiomyocyte isolations

Adult mouse cardiomyocytes (ACMs) were isolated as previously described[66]. In brief, mice were anesthetized with isoflurane and administered a 500 U heparin i.p. injection (Sigma Aldrich). Hearts were excised and cannulated within 4 min post excision on a Langendorff apparatus utilizing pH 7.4 perfusion buffer for 3 min comprising (mM, all from Sigma Aldrich): NaCl (120.4), KCl (12.7), KH_2PO_4 (0.6), Na_2HPO_4 (0.6), $MgSO_4$-7H2O (1.2), $NaHCO_3$ (4.6), Taurine (30), Glucose (5.5), 2,3-Butanedione 2-monoxime (BDM, 10), and HEPES (10). Perfusate was then switched to perfusion buffer including 2.4 mg/ml Type II Collagenase (Worthington Biochemical) followed with 3 μM $CaCl_2$ reintroduction when 20 mL of solution remain to perfuse. Aorta, vena cava, and atria were removed, and the ventricles were

mechanical broken apart into single cells. Cells were centrifuged at 30 x *g* for 3 min, and resuspended in three sequential stop buffers comprised of perfusion buffer and FBS + 10, 40, 100 μM $CaCl_2$ reintroduction steps were completed and cells were plated on dishes coated with 100 μg/ml laminin (Gibco) in cardiac myocyte media (CMM, ScienCell) with provided cardiac myocyte growth supplement, 5% FBS, 50 mM BDM, and MyocoZap Plus-PR (Lonza), which was replaced on cardiac myocytes at 2 h after plating.

Infections

In vivo

8-12 week old C57BL/6 male and female mice were anesthetized and inoculated via retro-orbital injection with 5×10^5 infectious units (i.u.) of MAdV-3 diluted in 0.9 % sterile saline (Teknova) or saline solution alone for control animals, using U-100 Insulin syringes (BD). Mice were monitored daily for weight loss and assessment of fur ruffling/neurological symptoms, none of which were noted in the work described herein.

In vitro

Infections were performed at a multiplicity of infection (M.O.I.) of 10 i.u./cell as previously described[38].

Echocardiography

Echocardiography was performed and analyzed using VisualSonics Vevo 660 High-Resolution Imaging System with a MS250 transducer at 7 days post-infection. Mice were anesthetized with 2 % isoflurane in 2 % supplemental O2 with long axis and M-mode images recorded, and surface electrodes measured cardiac electrical activity as previously reported[67]. Heart rate, electrocardiography, and left ventricle (LV) dimensions of ejection fractions (EF %), fractional shortening (FS %), left ventricular developed pressure (LVDP) at diastole were measured.

Histology

Histological preparation, blood counts, and serum chemistry analysis were performed according to standard operating procedures in the Virginia Tech Animal Laboratory Services (ViTALs) diagnostic laboratory accredited by the American Association of Veterinary Laboratory Diagnosticians (AAVLD) at Virginia-Maryland College of Veterinary Medicine. Tissues for histology were fixed in 10 % neutral buffered formalin (VWR) for 24 h, then trimmed, processed, paraffin-embedded, and sectioned at 5 μm prior to staining with hematoxylin and eosin (Abcam). Histopathologic examination was performed in a blinded fashion by a board-certified veterinary pathologist. Tissues evaluated included heart, brain, lungs, thymus, salivary glands, esophagus, tongue, eyes, spleen, adipose tissue, liver, kidneys, adrenal glands, pancreas, stomach, duodenum, jejunum, ileum, colon, skeletal muscle, bone, bone marrow, and haired skin.

Tissue DNA extraction and qPCR for viral genomes

Tissue was homogenized in TRIzol (Thermo Fisher) and DNA was extracted according to manufacturer's instructions in combination with ethanol precipitation. For detection of viral genomes, qPCR was performed with SYBR Select Master Mix for CFX (Thermo Fisher) on a QuantStudio 6 Flex System (Thermo Fisher). Cellular genome DNA reference gene C1 primer forward- 5'-CCT TCC AGT TGA GTC AGT GG-3' reverse- 5'-CTG CTG CTG TTG GGT ACT TC-3'. For detection of MAdV-3 viral genomes, MAdV-3 E1A primer forward- 5'-TCG TAC CCG CTT TTT CTG TT-3' reverse- 5'-AGG AGC AAT AAA AAT AAC CAA CCG-3' were employed.

RNA extraction and RT-qPCR

Tissue was homogenized in TRIzol (Thermo Fisher) and clarified by phenol-chloroform phase separation according to manufacturer's instructions. cDNA was generated with iScript Reverse

Transcription Supermix for RT-qPCR (Bio-Rad) according to manufacturer's instructions. Real-time PCR was performed with SYBR Select Master Mix for CFX (Thermo Fisher) on a QuantStudio 6 Flex System employing the following primers: *Gapdh*, Mm.PT.39a.1 IDT; *Hprt* Mm.PT.39a.22214828 IDT; *Cacna1c*, Mm.PT.58.8608981 IDT; *Scn5a*, Mm.PT.58.30418114 IDT; *Kcnh2*, Mm.PT.58.42865919 IDT; *Cdh2*, Mm.PT.58.12378183 IDT; *Pkp2*, Mm.PT.58.11914062 IDT; T*jp1*, Mm.PT.58.12952721 IDT; *Gja1*, Mm.PT.58.5955325 IDT; *Gjc1*, Mm.PT.58.8383900 IDT; *Gja5*, Forward: 5'-TAG ACA CCC AGC TCG TAA GG- 3' Reverse: 5'-GGT GAC TTT GGA CAT TCC TG -3'.

Langendorff heart preparations and optical mapping

Animals were anesthetized and cervical dislocation performed upon loss of peripheral stimuli response and immediately followed by thoracotomy and cardiac excision. Hearts were cannulated and Langendorff-perfused within 4 min, as previously described[68]. Hearts were perfused with a pH 7.4 baseline crystalloid solution containing (mM): NaCl (144.5), $CaCl_2$ (1.8), NaOH (5.5), KCl (4), Dextrose (5.5), $MgCl_2$ (1), HEPES (10), NaH_2PO_4 (1.2). Solutions were bubbled with 100% O2 for the duration of the experiment and run at a constant flow to maintain a pressure of ~70-90 mmHg, with perfusates and bath maintained at 37 °C. Following a 15 min stabilization period, hearts were perfused with 8 μM Di-4-ANEPPS (Biotium), excess dye was washed out over a 20 min period, and images acquired during subsequent perfusion. The electromechanical uncoupler blebbistatin (10 μM), as well as slight pressure on the posterior surface of the heart, were used to minimize cardiac motion and stabilize the heart against the glass of the imaging window. Hearts were paced with a unipolar silver wire placed on the anterior epicardium and a reference wire placed in the back of the bath. Stimulation of 1.5 X the threshold voltage was applied with a basic cycle length of 150 ms and 1 ms pulse duration. Hearts were paced for 30 sec before each image was collected. Action potentials were recorded as previously described[69]. Briefly, the anterior epicardium of the heart was exposed to a 520/35 nm band-pass filtered halogen light source (MHAB-150W, Moritex) reflected onto the heart via epi-illumination. Emitted light was collected via a tandem lens system and transmitted through a 610 nm long-pass filter (Andover Corp.) before detection with a MiCam Ultima L-type CMOS camera (SciMedia: 100 x 100 pixels, field of view – 6.25 x 6.25 mm). Action potentials were recorded at a sample rate of 1 kHz for a duration of 2 sec during intrinsic activity and steady state pacing. Conduction velocity (CV) was collected in the transverse and longitudinal direction (CVT and CVL, respectively), and was calculated as previously described[68]. Briefly, activation time for each pixel was designated as the maximum rate of rise of the optical action potential. Conduction in each direction was quantified by selecting vectors up to 5 pixels away and within an angle of ± 8° from a user-defined line indicating the direction of action potential propagation. Conduction vectors within 2 rows of the pacing site were excluded to reduce pacing artifacts. Data presented here are representative isochrone maps with 2 ms time steps.

Western blotting

Mouse hearts were homogenized in RIPA buffer (50 mM Tris pH 7.4, 150 mM NaCl, 1 mM EDTA, 1 % Triton X-100, 1 % sodium deoxycholate, 2 mM NaF, 200 μM Na_3VO_4, 0.1 % sodium dodecyl sulfate, 5 mM *N*-ethylmaleimide; all from Sigma Aldrich) supplemented with HALT protease and phosphatase inhibitor cocktail (Thermo Fisher). Lysates were clarified by sonication and centrifugation and concentration determined by DC protein assay (Bio-Rad). 4X Bolt LDS sample buffer (Thermo Fisher) supplemented with 400 mM DTT (Sigma Aldrich) was added to samples then heated to 70 °C for 10 min and subjected to SDS-PAGE using NuPAGE Bis-Tris 4-12 % gradient gels with MES (Thermo Fisher) running buffer according to manufacturer's instructions. Proteins were transferred to LF-PVDF (Bio-Rad) membrane and fixed in methanol and dried. PVDF membranes were reactivated in methanol followed by blocking in 5 % nonfat milk (Carnation) or 5 % bovine serum albumin (Fisher Scientific) in TNT

buffer (0.1 % Tween 20, 150 mM NaCl, 50 mM Tris pH 8.0) for 1 h at room temperature. Primary antibodies were incubated overnight at 4 °C utilizing: rabbit anti-Cx43 (1:3,000; Sigma-Aldrich), mouse anti-GAPDH (1:2,000; Santa Cruz Biotechnology), and rabbit anti-phospho-Cx43^{Ser368} [D6W8P] (1:1,000; Cell Signaling Technology). Membranes were washed six times with 1 X TNT before secondary antibody labeling. Membranes were labeled for 1 h at room temperature with secondary antibodies conjugated with AlexaFluor555 or AlexaFluor647 (1:5,000; Thermo Fisher) or HRP (1:5,000; Abcam). For HRP labeling (phosphor-Cx43^{Ser368}), membranes were stripped for 30 min in ReBlot Plus Strong Antibody Stripping Solution (Sigma Aldrich) before reprobing for total Cx43. Membranes were imaged utilizing a Chemidoc MP imaging system (Bio-Rad).

Patch clamping

Electrophysiological recordings from dissociated cardiomyocytes were performed at room temperature using whole-cell voltage-clamp and current-clamp techniques. Recordings were made with an Axopatch 200B amplifier, Digidata 1550B digitizer, and pClamp 11 software (Molecular Devices) with a 20 kHz sampling rate and low-pass filtering at 5 kHz. Series resistance was monitored and compensated at > 70 % during voltage-clamp recordings. Recording electrodes with a tip resistance of 2-4 MΩ were pulled from borosilicate glass. Action potentials and potassium currents (I_{K1}, I_{Ks}, and I_{Kr}) were recorded with an internal pipette solution containing (mM): K-aspartic acid (120), KCl (20), NaCl (10), $MgCl_2$ (2), and HEPES (5) brought to pH 7.3 with KOH, and extracellular solution containing (mM): NaCl (120.4), KCl (12.7), KH_2PO_4 (0.6), Na_2HPO_4 (0.6), $MgSO_4$-$7H_2O$ (1.2), $NaHCO_3$ (4.6), Taurine (30), Glucose (5.5), and HEPES (10) brought to pH 7.4 with HCl. Sodium current and calcium currents were recorded with an internal pipette solution containing (mM): $CsMeSO_3$(120), tetraethylammonium chloride (20), $MgCl_2$ (2), HEPES (10), EGTA (10), and Mg-ATP (4) brought to pH 7.3 with CsOH. Sodium currents were recorded in extracellular solution containing (mM): NaCl (25), N-methyl-D-glucamine (120), $CaCl_2$ (1.8), $MgCl_2$ (1.8), glucose (10), and HEPES (10), pH 7.3, supplemented with 1 μM nisodipine to block voltage-gated calcium channels. Calcium currents were recorded in extracellular solution containing (mM): NaCl (137), CsCl (5.4), $MgCl_2$ (1.8), $CaCl_2$ (2), glucose (10), and HEPES (10), pH 7.3, supplemented with 10 μM TTX to block voltage-gated sodium channels.

Action potentials were recorded in current-clamp mode and elicited by a 2 ms current pulses between 200 pA to 2 nA at 1 sec intervals. Action potential shape analysis was performed on action potentials elicited in response to the lowest current injection using the Action Potential module in Clampfit 11 (Molecular Devices). I_K, I_{Na}, and I_{Ca} were recorded in voltage-clamp mode, and the 10 mV liquid junction potential was corrected for during the recordings. I_{K1} was elicited from a holding potential of -40 mV with 2.5 sec depolarizing voltage steps from -100 mV to 0 mV and quantified by measuring the peak steady-state current amplitude during the voltage steps. To measure I_{Ks} and I_{Kr}, cardiomyocytes were held at a holding potential of -40 mV holding potential, given depolarizing voltage pulses from -30 to 60 mV for 2.5 sec, and then stepped back to -40 mV in the absence and presence of 5 μM E4031 (Cayman chemical). I_{Ks} was determined by measuring the peak amplitude of the tail current in the presence of E4031, and I_{Kr} was determined by measuring the peak amplitude of the E4031-sensitive current. I_{Na} was elicited from a holding potential of -90 mV with 20 ms depolarizing steps from -80 mV to +60 mV. I_{Ca} was recorded from a holding potential of -40 mV with 300 ms depolarizing steps from -30 mV to +60 mV. I_{Na} and I_{Ca} were determined by measuring the peak current amplitude relative to baseline during the voltage steps. Three runs were completed per cell for all recordings.

Immunofluorescence microscopy
As previously described[38,70,71] cells were fixed with -20 °C methanol for 5 min, washed, and blocked with 5 % normal goat or donkey serum (Thermo Fisher) containing 0.1 % Triton X-100 (Sigma Aldrich) which was increased to 0.5 % for ACMs for 1 h at room temperature. Primary antibody labeling was performed for 1 h at room temperature using; rabbit anti-Cx43 (1:3000; Sigma), mouse anti-N-Cadherin (1:750; Cell Signaling Technology), mouse anti-Adenovirus E1A [M73] (1:2000; Abcam). Cells was washed 6 times prior to labeling for 1 h at room temperature with AlexaFlour-conjugated secondary antibodies raised in goat (1:500, Thermo Fisher) and counterstained with DAPI (1:1000; Thermo Fisher). Confocal imaging was performed on Nikon SoRa Spinning Disk confocal and image processing was done in FIJI software (NIH)[72].

Live calcium transients imaging
HiPSC-CMs were plated into 35 mm glass bottom culture dishes (Cellvis) and maintained as described above to form monolayers and mature. Cells were infected with HAdV-5 at an MOI of 10 and loaded with Fluo-4AM (Thermo Fisher) diluted in Tyrode's solution containing (mmol/L): NaCl (140), KCl (5.4), $MgCl_2$ (1), sodium pyruvate (2), $CaCl_2$ (1), glucose (10), HEPES (10), pH adjusted to 7.4 using NaOH at room temperature[73]. Live cell imaging was performed utilizing an Opterra swept field confocal microscope (Bruker) with a 20x objective with an acquisition rate of 166.67 Hz for at least 6 fields of view per well encompassing several spontaneous firings. Fluorescence from image sequences encompassing one field of view was normalized in FIJI[72] by generating maximum (MaxIP) and minimum (MinIP) intensity projections, and subtracting MinIP from the original image sequence and MaxIP. The resulting image sequence was divided by the result of MaxIP/MinIP. Regions of interest were defined over individual cells and fluorescence intensity plotted over time. Standard deviation of timepoint for peak fluorescence intensity of one firing from 4 cells in each sequence was calculated as a measure of synchronicity.

Statistics
All experiments were repeated at least three times and blinding of data was implemented prior to quantification (see figure legends for specific replicate values). Data are presented as mean ± SEM. Statistical analysis was conducted with GraphPad Prism (GraphPad Software, Inc.). Data were analyzed for significance using Student's t-test or one-way ANOVA correcting for multiple comparisons. A value of $p<0.05$ was considered statistically significant.

Results

Mouse adenovirus type-3 is cardiotropic and does not invoke an appreciable immune response or cardiomyopathy during acute infection.

We previously reported specific targeting of Cx43 expression and gap junction function during adenoviral infection[38]. Such alterations in Cx43 would significantly impact cardiac electrophysiology directly through affecting GJIC, while potentially indirectly impacting sodium channels and/or other key components of arrhythmogenesis[19,21,74,75]. Despite significant incidence of adenoviral myocarditis, establishment of an adult mouse disease model has been elusive due to species-specificity[54]. We first sought to examine the potential of MAdV-3 as a model of acute cardiac infection, given the prior reports of cardiotropism[59]. To test this, 8-12 week old male and female C57BL/6 mice were inoculated with 5 x 10^5 i.u. MadV-3 via retro-orbital injection. Animals were sacrificed and organs harvested 7 d.p.i. for histology and DNA isolation. Using qPCR we find MadV-3 viral genomes enriched only within cardiac tissue (fold change of heart compared to lung ± standard error of the difference: 75.77 ± 9.521, brain; 77.02 ± 9.814, kidney; 73.52 ± 9.521, intestine; 76.68 ± 9.521, pancreas; 74.94 ± 10.65, skeletal muscle; 76.96 ± 9.814, liver; 75.06 ± 9.078, and spleen; 68.36 ± 9.521; Comparisons between all other organs are not significant), confirming cardiotropism (Figure 1A). A similar time-course over 7 days focusing on cardiac tissue alone reveals levels of viral genomes plateauing from 3-7 d.p.i., consistent with active viral replication in the heart during this time (Figure 1B). No weight loss or apparent evidence of malaise (e.g. hunching, fur-ruffling) were observed in infected animals during the 7 day time course (data not shown). Turning to cardiac function, we find no detectable changes in ejection fraction, left ventricle developed pressure at diastole, or fractional shortening by echocardiography in infected animals compared to controls (Figure 1C). Histopathology reveled no gross pathology or appreciable infiltration of leukocytes in infected cardiac tissue (Figure 1D). This lack of direct cardiomyocyte damage and presence of a cardiac inflammatory response were confirmed by serum cardiac troponin I (cTnI) ELISA and cytokine array on heart protein lysates, respectively, where no significant changes were detected between groups (Supplemental Figure 1A, Supplemental Figure 2). Gross spleen weight, however, was higher in infected mice (83.3 ± 5.58 mg vs.133.5 ± 7.45 mg, mean ± SEM), in addition to increased spleen node size, indicative of initiation of the adaptive immune response (Supplemental Figure 1B, C). Together, these findings confirm that MAdV-3 is cardiotropic, representing a relevant model of acute viral myocarditis to examine mechanisms of arrhythmogenesis prior to appreciable host immune-involvement or cardiomyopathy, and faithful to reported presentation of such cardiac infections in humans[8].

Cardiac conduction velocity is slowed during acute adenoviral infection.

Data in Figure 1 confirm MAdV-3 cardiotropism in mice, and identify 7 d.p.i. as a timepoint where viral replication has been occurring in the heart for several days while detectable immune infiltration and/or cardiomyopathy have not yet occurred. Given cases of SCD with acute viral involvement often involve essentially normal heart structure at the gross level, we next asked how cardiac electrophysiology may be affected during MAdV-3 infection. Infected and control animals were anesthetized and, using electrode pads, baseline ECGs revealed no alterations to the PR, QRS, or QT intervals in MAdV-3-infected mice compared to mock-infected animals (Figure 2A-D). A significant prolongation of the R-R interval (114.4 ± 0.98 ms, MAdV-3 infected mean 121.4 ± 1.77 ms, mean ± SEM, Student's t-test, $p<0.01$), indicative of bradycardia, was detected in infected animals, however (Figure 2E). To assess alterations in intercellular coupling, we next turned to measurement of conduction velocity (CV) by optical mapping. Excised hearts from infected and control animals were Langendorff-perfused and optical mapping performed to quantify longitudinal and transverse CV (CVL and CVT, respectively) during steady-state perfusion (Figure 3). While CVL was similar in both groups, we find

significant CVT slowing in MAdV-3-infected hearts in comparison to mock-infected controls (38.75 ± 2.60 vs. 29.33 ± 2.88 cm/s, mean ± SEM, respectively: Figure 3C). Such reductions in ventricular conduction velocity are known to underlie arrhythmogenesis and mechanistically are typically associated with perturbation of gap junction function and/or connexin expression[17,74,76-80].

Aberrant connexin43 expression and phosphorylation are induced in MAdV-3 infected hearts.

Having identified a conduction defect in MAdV-3 infected hearts, we next examined expression of proteins critical to cardiomyocyte ID structure and gap junction formation and maintenance. Using cDNA generated from MAdV-3 infected or control ventricular tissue, mRNA levels of the major cardiac gap junction and junctional/scaffolding proteins were quantified by RT-qPCR. Transcript levels of *Cdh2* (N-cadherin) and *Tjp1* (ZO-1) were reduced in infected hearts (*Cdh2*: 1.049 ± 0.179, vs. 0.1629 ± 0.069, *Tjp1*: 1.121 ± 0.260 vs. 0.2832 ± 0.101, mean ± SEM) along with gap junction genes *Gja1* (Cx43) and *Gjc1* (Cx45) (*Gja1* 1.058 ± 0.217 vs. 0.1416 ± 0.056, *Gjc1* 1.122 ± 0.257 vs. 0.2264 ± 0.084, mean ± SEM) while *Pkp2* (plakophilin 2) and *Gja5* (Cx40) were not significantly altered (Figure 4A, Supplemental Figure 3). Previously, we found a decrease of Cx43 protein localization at the cell-cell border during HAdV-5 infection in HaCaT and HiPSC-CMs[38]. To ask if gap junction localization at the ID was affected in MAdV-3 infected mouse hearts, we performed confocal immunofluorescence microscopy on myocardial cryosections to visualize Cx43 distribution in ventricular cardiomyocytes. Through quantification of Cx43 intensity at the ID, as determined through colocalization with N-cadherin[26,71,81], we find no significant losses in gap junction localization between infected or control hearts (Figure 4B). While *Gja1* mRNA was reduced in infected hearts (Figure 4A), levels of Cx43 protein were comparable by western blotting of lysates from MAdV-3 infected versus control cardiac tissue lysates at 7 d.p.i. (Figure 4C). Given our finding of slowed CVT without detectable alterations in Cx43 protein expression or localization, we assessed the post-translational status Cx43. Specifically, phosphorylation of $Cx43^{Ser368}$ results in reduced channel opening probability, and our prior work with HAdV-5 identified this residue as being hyperphosphorylated during infection of human epithelial cells[29,30,38]. Consistent with this, we find induction of $Cx43^{Ser368}$ phosphorylation by western blotting of ventricular lysate from mice infected 7 d.p.i. with MAdV-3 in comparison to mock-infected animals (0.3731 ± 0.044 vs. 0.6515 ± 0.115, mean ± SEM) (Figure 4D).

Adenoviral infection prolongs adult cardiomyocyte action potential duration through perturbation of potassium currents.

Proper cardiac electrophysiology depends not just upon intercellular coupling and AP propagation, but the repetitive formation and resolution of consistent AP morphology through the dynamic actions of several ion channels[12]. Examining ion channel candidate genes by RT-qPCR we do find significant reductions in mRNA transcripts of *Cacna1c* ($Ca_V1.2$) and *Scn5a* ($Na_V1.5$) in MAdV-3 infected hearts 7 d.p.i. when compared to controls, (*Cacna1c*: 1.379 ± 0.46 vs. 0.3720 ± 0.125, *Scn5a*: 1.138 ± 0.057 vs 0.9916 ± 0.309, mean ± SEM) but no detectable change to *Kcnh2* (hERG) expression (1.652 ± 0.794, 0.7570 ± 0.277, mean ± SEM) (Figure 5A). Given the discrepancy we detected between *Gja1* mRNA reduction with no change to Cx43 protein levels, but significantly altered GJ function in infected hearts (Figure 3, Figure 4), we next turned to patch-clamping as a non-biased approach in measuring changes to cardiomyocyte electrophysiology during infection. Primary adult mouse ventricular cardiomyocytes were infected immediately post-isolation with MAdV-3 at a multiplicity of infection (MOI) of 10 or mock-infected and incubated for 24 h prior to experimentation. Importantly, infected cells were viable at this timepoint with no apparent cytopathic effect noted.

Using confocal immunofluorescence microscopy, 100% infection was confirmed using MAdV-3 antiserum, where infected cells are noted to have maintained normal structure (data not shown). First, we performed whole-cell current clamp to determine if AP morphology was altered during MAdV-3 infection. While no alterations in depolarization rate (rise time/max rise slope) were detected, significant AP duration (APD) prolongation occurs in MAdV-3 infected cells relative to uninfected controls presented here through increased APD90 (13.87 ± 0.633 ms vs. 17.02 ± 0.674 ms, mean ± SEM) and decay time (6.028 ± 0.314 ms, 8.598 ± 0.567 ms, mean ± SEM) concomitant with decreases in max decay slope (-34.31 ± 2.817 ms vs. -26.17 ± 1.902 ms, mean ± SEM) and afterpolarization (AHP) amplitude (-1.919 ± 0.199 mV vs. -1.287 ± 0.193 mV, mean ± SEM) (Figure 5B-E). Having identified such pathological APD prolongation, we next utilized whole-cell voltage-clamp to assess individual currents and isolate the specific cardiomyocyte ion channels affected during MAdV-3 infection. Despite reduced mRNA transcripts of *Cacna1c* and *Scn5a* in infected hearts (Figure 5A), no alterations in I_{Na} or I_{Ca} were detected in MAdV-3 infected ACMs (Figure 6A,B). The AP morphology changes we report occur during phases 3 and 4 however, leading us to focus in more detail on the potassium currents which primarily control proper repolarization and AP resolution. While no difference in I_{Kr}, or I_{Ks} peak currents were detected between control and infected ACMs, I_{Ks} tail current differences (50 mV; -4.504 ± 0.639 pA/pF vs -3.149 ± 0.532 pA/pF, 55 mV; -5.033 ± 0.582 pA/pF vs. -3.159 ± 0.529 pA/pF, 60 mV; -4.034 ± 0.556 pA/pF MAdV-3 mean average -3.271 ± 0.523 pA/pF, mean difference ± SEM) and I_{K1} peak current (-19.80 ±1.989 pA/pF vs. -12.24 ± 1.612 pA/pF, mean ± SEM) were significantly perturbed during MAdV-3 infection (Figure 6C-E, Supplemental Figure 4). These data reveal potentially arrhythmogenic APD prolongation occurs in infected ventricular cardiomyocytes, compounding the electrophysiological disturbances we report affecting conduction velocity and cardiac GJ function during acute MAdV-3 infection of the heart.

Human Adenovirus Type-5 increases Cx43^{Ser368} phosphorylation and uncouples HiPSC-derived cardiomyocytes.

We previously reported that HAdV-5 disrupts expression and function of Cx43 in human epithelial cells and complexing of Cx43 with ZO-1 in HiPSC-CMs[38]. To translate our current findings of GJIC disruption and CV slowing in MAdV-3 infected mouse hearts (Figure 3, Figure 4) to a human model system, we investigated how functional intercellular coupling might be altered in HAdV-5 infected HiPSC-CMs. Matured HiPSC-CM were cultured and infected with human adenovirus type-5 (HAdV-5) or with HAdV-LacZ, a replication incompetent human adenovirus serving as control, at an MOI of 10. Cells were lysed and western blotting performed 24 h.p.i. where we find significant induction of Cx43^{Ser368} phosphorylation in HAdV-5 infected cells (0.06382 ± 0.005 vs. 0.1265 ± 0.004, mean ± SEM) (Figure 7A), consistent with what we report in MAdV-3 infected mouse heart tissue (Figure 4D). To assess the impact of infection on electrical coupling, monolayers were loaded with the calcium sensitive Fluo4-AM 24 h.p.i. and live-cell confocal microscopy performed at 166 Hz to visualize spontaneous calcium transients. After imaging, cells were fixed and 100% infection confirmed through immunofluorescence labeling of the early HAdV-5 protein E1A (Figure 7B). While HAdV-LacZ (control) HiPSC-CMs consistently displayed synchronous firing across the monolayer, uncoupling of HAdV-5 infected cells is demonstrated through significant cell-to-cell variability in time to max peak intensity (53.17 ± 8.426 ms vs. 123.8 ± 23.930 ms, mean ± SEM) (Figure C,D). Therefore, just as we find in our MAdV-3 in vivo and in vitro studies, HAdV-5 infection disrupts cardiomyocyte electrical coupling independent of a significant infiltrative immune response, confirming that acute adenoviral infection generates dangerous electrical disturbances in still-viable cardiomyocytes which likely contribute to the arrhythmias of SCD attributed to acute viral myocarditis.

Discussion

By definition, viral myocarditis encompasses inflammation and a significant contribution to either gross or molecular myocardial alterations due to infiltration of host immune cells and associated cytokine signaling[82]. There is, however, a significant gap in our understanding of pathologic events that occur during acute cardiac infection, prior to development of any detectable cardiomyopathy or mounting the infiltrative host antiviral immune response[83]. In this study, we implement MAdV-3 as a model cardiotropic adenovirus to isolate virally induced mechanisms of arrhythmogenesis during initial/acute infection that precede myocarditis or chronic disease development. While historically understudied in the context of cardiovascular disease, adenoviruses are a leading causative agent of myocarditis with the majority of cases seemingly reported in young adults and children[84]. Moreover, adenoviral genomes have been detected in cardiac tissue in cases of SCD where gross structural changes of the myocardium are not apparant[85]. We report that, prior to an appreciable immune response in cardiac tissue; adenoviral infection decreases potassium current density leading to prolonged action potential duration with concurrent reductions in gap junction intercellular communication affecting conduction.

Viruses hijack cell machinery to enable their replication while hindering host cellular and organismal immune responses[86,87]. Previous research has demonstrated that cGAS, a key signaling molecule in the innate and cell-intrinsic interferon antiviral immune response, can pass via gap junctions from infected cells to uninfected neighbors, priming and propagating the antiviral state[35]. Additionally, adaptive antiviral immune responses can be amplified in this manner by means of short linear peptide exchange via gap junctions effecting presentation of viral antigens on HLA complexes of uninfected neighboring cells that cytotoxic CD8 T-cells can engage[36]. Previously, we have reported that human adenoviral E4-ORF1 can decrease Cx43 protein expression through transcriptional repression via β-catenin, resulting in decreased gap junction intercellular communication in human epithelial cell[38]. In addition to reduced Cx43 expression, we found an increase in phosphorylation of Cx43 C-terminal sites known to be modified by AKT and PKC, retaining Cx43 at the cell membrane and reducing GJIC in cells infected with HAdV-5[38]. In this current study, we build on these findings by investigating the effects of viral modification of GJIC in the whole heart using a cardiotropic adenovirus to better understand the role of infection in precipitation of the arrhythmogenic substrate.

Consistent with our prior findings, new data from HAdV-5 infected human iPSC-CMs *in vitro* and MAdV-3 *in vivo* infections, reveal similar induction of $Cx43^{Ser368}$ phosphorylation with concurrent reductions in gap junction function (Figure 4, Figure 7). These data demonstrate a conserved mechanism between human and mouse adenoviral infection occurring across diverse infected cellular populations (epithelial cells and cardiomyocytes) to rapidly limit intercellular communication. Perturbed gap junction coupling during adenoviral infection of the lung epithelium would presumably have limited serious pathological implications for the host. Regarding infection of the working myocardium however, such rapid disruptions in intercellular communication would likely precipitate arrhythmias of SCD during acute infection. Our data support this scenario, whereby we find $Cx43^{Ser368}$ phosphorylation occurs in concert with both uncoupling of, and altered calcium handling in, iPSC-CMs *in vitro*, and decreased conduction velocity *in vivo* (Figure 3, Figure 7). Indeed, Huke et al. reported a relationship between reduced intercellular coupling of cardiomyocytes, the development of focal arrhythmias, and increased Cx43 phosphorylation[88].

Slowed conduction velocity is a well-known arrhythmogenic determinant and is closely linked to gap junction function in the heart expression[17,74,76-80]. Previous reports have demonstrated that

uncoupling of cardiomyocytes favors a decreased conduction velocity in the transverse direction[89,90]. This phenomenon is due to the higher density of gap junctions per a myocyte area in the transverse direction, as such, the increased intercellular junctions at a given area result in increased resistance, and decreased velocity[91-93]. Thus, the reductions in conduction velocity in the transverse direction point to loss and/or alteration of gap junction function and can precipitate arrhythmias. This propensity supports our observations of a decrease of CVT in infected mice but no change in CVL as being due to gap junction dysfunction (Figure 3). Other viral agents have been shown to alter intercellular communication by way of phosphorylation of connexins during infection. Various viruses are known to decrease intercellular communication during disease, such as herpes simplex virus (HSV), feline immunodeficiency virus, and bovine papillomavirus[94-96]. Herpes simplex virus type-2 infection in rat liver epithelial cells increased serine phosphorylation 24 h.p.i. and reduce GJIC, resulting in eventual loss of Cx43 localization at the membrane[96]. In murine fibroblasts, Rous sarcoma virus, an oncogenic virus, increased phosphotyrosine and phosphoserine and reduced GJIC[97]. Human papillomavirus 16 (HPV16) protein E6 has been found to sequester Cx43 in the cytosol, limiting trafficking and gap junction formation, and potentially facilitating tumor progression. Although not directly tested, the authors report altered Cx43 phosphorylation as a likely mechanism by which HPV16 E6 achieves this[98]. While changes to connexin phosphorylation caused by acute viral infection is most commonly studied in the context of cancer biology, clearly such changes to gap junction phosphorylation will also impact cardiomyocyte coupling across a variety of viral infections.

Adenoviral infection rapidly alters host-signaling cascades to facilitate viral invasion and replication[99,100]. Our findings of decreased conduction velocity and increased phosphorylation at $Cx43^{Ser368}$ in the heart during adenovirus infection are in line with previous research of the interplay between viruses and PKC signaling[101,102]. For example, early in infection increased expression of adenoviral protein E1A correlates with increased PKC levels, a family of kinases whose activity is required for viral endosome escape[103,104]. Adenoviral E1A is the first protein expressed in the adenoviral life cycle and increased E1A correlates with elevated levels of viral protein along with increased PKC protein[104]. However, the E1A activation of PKC signaling in adenoviral early infection needs further delineation. PKC and downstream protein signaling regulate the cell cycle, which has been well-studied in both the fields of cancer and immune cell proliferation[105,106]. PKC exerts control over many cyclin genes, a particular note Cyclin D, via transcription and thus can uncouple cells to start cell cycle from S phase[107]. Adenoviruses push cells into S phase via E1A, E1B, and E4 protein interaction with host mechanisms, and this is required for viral replication[108-110]. Cardiomyocytes, themselves, are typically quiescent several days after birth, and therefore, are particularly recalcitrant to entering the cell cycle[111]. We must also now consider how activation of these signaling pathways shuts down gap junction intercellular communication in addition to facilitating S-phase entry. Therefore, acute adenoviral infection of the myocardium likely causes arrhythmogenesis via activation of AKT/PKC pathways which impact Cx43, and potentially other critical cardiac ion channel function.

In addition to gap junction disruption, our data provide evidence that adenoviral infection prolongs action potential duration through limiting I_{K1} and I_{Ks} in adult ventricular cardiomyocytes. Ventricular electrophysiology is therefore likely further compromised in addition to conduction delay in infected hearts (Figure 5, Figure 6). Prolonged action potential duration (APD) can precipitate an arrhythmogenic substrate through early and/or delayed afterdepolarization in cardiomyocytes, leading to tachycardia/fibrillation[112]. The APD is determined by several distinct cardiomyocyte ionic currents such as sodium (I_{Na}), calcium (I_{Ca}), together with several potassium currents including I_{K1}, I_{Kr}, and I_{Ks}. There is, however, a paucity of data regarding the effects of viral infection on action potential duration. Turning to models of Long QT syndromes (LQT), we can interpret how alterations to these currents contribute to sudden cardiac arrest. Anderson-Tawil syndrome

(LQT7) is caused by a monogenic defect in KCNJ2 and presents as ventricular arrhythmias, prolonged QT intervals, together with physical malformations[113,114]. The ventricular arrhythmias in LQT7 are due to defects in KCNJ2, the protein responsible for the Kir2.1 inward rectifier K+ current of I_{K1}, which lead to spontaneous action potential durations and early/delayed afterdepolarizations[114-116]. The KCNQ1 and KCNE1 proteins form the $K_V7.1$ channel, creating the slow activating delayed rectifier current, I_{Ks}[117]. Genetic modeling of LQT1 syndrome by loss-of-function in KCNQ1 causes decreased I_{Ks} that underlies ventricular arrhythmias and SCD[118]. Several mutations causing LQT1 impair trafficking of KCNQ1 to the cell surface, which could inform future directions in understanding the effects on I_{Ks} we have identified during acute adenoviral infection[119].

Specific targeting of ion channel function has previously been described across various viral species and host cell types. In a cardiac model, CVB3 viral titers were increased in the *mayday* mutant mouse model; these mice are deficient in Kir6.1, a subunit of KATP channels, and had decreased survivability after infection[120,121]. Turning to non-cardiac excitable tissues, patch clamping experiments of neuroblastoma cells that were infected with rabies virus displayed decreased I_{Kir} and I_{Na} amplitude 3 d.p.i with no observable morphological changes[122]. While many of these studies lack a viral mechanistic cause of the change in K+ currents, it is plausible to consider this as a viral advantage, as viruses across different realms clearly and specifically alter such ionic currents during infection. Potassium channels are ubiquitously found across almost all cell types, including non-excitable cells. This included the epithelium, a common entry point for most viruses, and other cell types such as immune cells, such as macrophages and T-cells[123-126]. Interestingly, K+ channels in the epithelium are localized along the basolateral membrane, coincident with the Coxsackie adenovirus receptor (CAR) and integrins utilized by human adenoviruses for entry[124].

Could a common mechanism underlie the arrhythmogenic alterations to gap junctions and K+ currents we report? PKC is known to phosphorylate a multitude of host proteins relevant to our findings, including $K_V7.1$ and Cx43[31]. As the kinase responsible for phosphorylation of $Cx43^{Ser368}$, PKC activation is well-described in subsequent reduced gap junction channel opening probability[29,30,127]. PKC signaling is also known to regulate I_{Ks} by promoting $K_V7.1$ endocytosis through increased phosphorylation of KCNE1[31]. When broadly looking at the role of kinases during ischemic stress and heart failure, PKC signaling has been found to be sufficient in I_{K1} reduction[128]. The commonality between negative regulation of Cx43 and I_{K1} and I_{Ks} currents by PKC strongly implicates it as a potential central kinase activated during viral infection that concurrently, and dangerously, affects distinct arms of cardiac electrophysiology. Given that PKC isoforms are known to regulate many endosomal functions, such as endocytosis and trafficking from the membrane, it is unsurprising that many viruses target this pathway for host cell invasion[129]. The direct interaction with PKC family members is vital for influenza assembly, replication machinery function, and endosomal exit[130,131]. For example, West Nile virus replication is inhibited when PKC activity is blocked and viral fusion of Respiratory Syncytial Virus (RSV) requires PKCα membrane translocation[101,132]. Thus, modification of the PKC family is a common mechanistic target across viral families.

The question remains as to how and why a DNA tumor virus such as adenovirus would infect terminally differentiated muscle, such as in the working myocardium. As mentioned above, adenoviruses induce cell cycle entry to facilitate their own genome replication by arresting infected cells in S-phase[45]. Given their recalcitrance to cell cycle entry, compared to epithelial cells, it is tempting to speculate that adult cardiomyocytes are not the intended host cell for adenovirus, but when infected, precipitate an unfortunate and potentially deadly pathological process. Human adenoviruses are understood to primarily utilize CAR for binding and host cell

entry, just like CVB3, although CAR-independent infection is also reported[60,133-135]. A component of the intercellular junction, CAR is expressed in several tissue types, including the heart, where it is primarily expressed on endothelial, epithelial cells, and at the cardiomyocyte ID[136,137]. In cardiomyocytes, CAR appears to play an integral role in coupling cells together for electromechanical and metabolic signaling[138,139]. The enrichment of CAR in the heart may, in part, contribute to adenoviral infection and colonization of this tissue should viremia occur, for example.

Aside from the significant body of viral myocarditis research employing CVB3, reovirus has also been developed as a model which, while typically not causing disease in humans, elicits myocarditis in neonatal mice[140]. Acute reovirus infection causes cytopathic effect specifically in cardiomyocytes, as compared to fibroblasts or epithelial cells[141]. This increases inflammation and infiltration of host immune cells, which is a common pathogenesis to that reported in CVB3 infection[142]. Mouse adenovirus Type-1 (MAdV-1) has previously been employed to investigate adenoviral-specific cardiac infection. The Weinberg group has shown significant inflammation of cardiac tissue, immune cell infiltration, and cardiac output during chronic MAdV-1 infection[55,56]. This response occurred along with high levels of IFN-γ and the immunoproteasome induced in a dose-dependent and inverse age-dependent manner that followed IFN-γ levels[55,56,143]. These models are beneficial to understand the role of direct and indirect immune-mediated responses in the heart during infection with a virus that also afflicts the respiratory system[144]. Together, while this research has contributed much to our understanding of viral-mediated inflammation of the heart, previous studies demonstrate that there are pathogen-specific effects to the host cell at the molecular level, especially relevant to acute stages of myocarditis[83]

As acute infections are hypothesized to be a significant cause of sudden cardiac arrest, we sought to employ MAdV-3 as a novel acute adenoviral myocarditis model. Through studying the infected heart at early stages of viral colonization and replication, we have revealed previously underappreciated effects of viral-mediated changes to cardiomyocytes precipitating electrophysiological defects and leading to an arrhythmogenic substrate. Overall, there has been a paucity of research into direct adenoviral mechanisms that induce arrhythmogenesis and our data introduce MAdV-3 infection as a viable model with which to study adenoviral cardiac infection and myocarditis progression in the adult mouse. Relevance to human disease is confirmed through complementary work in HiPSC-CMs and HAdV-5 where we find infected cardiomyocytes undergo arrhythmogenic alterations to intercellular coupling and electrophysiology while still viable, and in the absence of an inflammatory or adaptive host immune system. Clinical relevance is also confirmed through our *in vivo* studies where, just as in human patients, we uncover an arrhythmogenic substrate in infected hearts which are free of any remarkable cardiomyopathy or inflammation[8]. These data provide insight not just into mechanisms of arrhythmogenesis during acute cardiac adenoviral infection, but also the state of key players in cardiac electrophysiology in phases of disease preceding gross remodeling of myocarditis and progression to heart failure. In addition to informing therapeutic interventions, the ability to model acute cardiac infection will facilitate development of diagnostic approaches to identify at-risk individuals with limited clinical presentation by current screening/imaging methods.

Acknowledgments
The authors thank Dr. Sarah Barrett (Virginia-Maryland College of Veterinary Medicine) for undertaking histopathology. This work was supported by NIH NHLBI R01 grants: HL132236 and HL159512 to J.W.S.; HL138003 and HL141855 to S.P., NINDS R01 grant NS105804 to S.A.S., and NHLBI F31 grants: HL152649 to R.L.P.; HL160172 to G.A.B.; HL147438 to D.R.K.

Author contributions
J.W.S. and R.L.P. designed this study. R.L.P. performed cell and animal infections, viral propagation, primary cell isolations, RT-qPCR, qPCR, confocal, western blotting, troponin ELISA, live cell imagining, echocardiography experiments and analysis. G.A.B. performed the optical mapping and analysis. M.D.N. performed cryosectioning and confocal immunofluorescence microscopy. M.J.Z. differentiated and cultured HiPSC-CMs and assisted in all data analyses. M.T.T. performed and analyzed the echocardiograms. D.R.K. and G.S.H. assisted in design and analysis of optical mapping and electrophysiology experiments. S.A.S. performed and analyzed the patch clamping experiments. S.P. provided electrophysiology experimental design, data analysis and manuscript feedback. J.W.S. supervised all work and performed the cytokine array and live cell imaging analysis. J.W.S. and R.L.P. analyzed the data and interpretation. R.L.P. wrote the manuscript with J.W.S.

Declaration of interests
The authors declare no competing interests.

References

1. Babu-Narayan SV, McCarthy KP, Ho SY, Magee AG, Kilner PJ, Sheppard MN. Images in cardiovascular medicine. Myocarditis and sudden cardiac death in the young: extensive fibrosis suggested by cardiovascular magnetic resonance in vivo and confirmed post mortem. *Circulation*. 2007;116:e122-125. doi: 10.1161/CIRCULATIONAHA.107.693085
2. Dennert R, Crijns HJ, Heymans S. Acute viral myocarditis. *Eur Heart J*. 2008;29:2073-2082. doi: 10.1093/eurheartj/ehn296
3. Baksi AJ, Kanaganayagam GS, Prasad SK. Arrhythmias in viral myocarditis and pericarditis. *Card Electrophysiol Clin*. 2015;7:269-281. doi: 10.1016/j.ccep.2015.03.009
4. Woodruff JF. Viral myocarditis. A review. *The American journal of pathology*. 1980;101:425-484.
5. Blauwet LA, Cooper LT. Myocarditis. *Prog Cardiovasc Dis*. 2010;52:274-288. doi: 10.1016/j.pcad.2009.11.006
6. Kuhl U, Pauschinger M, Seeberg B, Lassner D, Noutsias M, Poller W, Schultheiss HP. Viral persistence in the myocardium is associated with progressive cardiac dysfunction. *Circulation*. 2005;112:1965-1970. doi: 10.1161/CIRCULATIONAHA.105.548156
7. Tschope C, Ammirati E, Bozkurt B, Caforio ALP, Cooper LT, Felix SB, Hare JM, Heidecker B, Heymans S, Hubner N, et al. Myocarditis and inflammatory cardiomyopathy: current evidence and future directions. *Nat Rev Cardiol*. 2021;18:169-193. doi: 10.1038/s41569-020-00435-x
8. Ammirati E, Cipriani M, Moro C, Raineri C, Pini D, Sormani P, Mantovani R, Varrenti M, Pedrotti P, Conca C, et al. Clinical Presentation and Outcome in a Contemporary Cohort of Patients With Acute Myocarditis: Multicenter Lombardy Registry. *Circulation*. 2018;138:1088-1099. doi: 10.1161/CIRCULATIONAHA.118.035319
9. Leoni D, Rello J. Cardiac arrest among patients with infections: causes, clinical practice and research implications. *Clin Microbiol Infect*. 2017;23:730-735. doi: 10.1016/j.cmi.2016.11.018
10. Harris KM, Mackey-Bojack S, Bennett M, Nwaudo D, Duncanson E, Maron BJ. Sudden Unexpected Death Due to Myocarditis in Young People, Including Athletes. *Am J Cardiol*. 2021;143:131-134. doi: 10.1016/j.amjcard.2020.12.028
11. Liberthson RR. Sudden death from cardiac causes in children and young adults. *N Engl J Med*. 1996;334:1039-1044. doi: 10.1056/NEJM199604183341607
12. Grant AO. Cardiac ion channels. *Circ Arrhythm Electrophysiol*. 2009;2:185-194. doi: 10.1161/CIRCEP.108.789081
13. Kurtenbach S, Kurtenbach S, Zoidl G. Gap junction modulation and its implications for heart function. *Front Physiol*. 2014;5:82. doi: 10.3389/fphys.2014.00082
14. Smyth JW, Shaw RM. The gap junction life cycle. *Heart Rhythm*. 2012;9:151-153. doi: 10.1016/j.hrthm.2011.07.028
15. Nattel S, Maguy A, Le Bouter S, Yeh YH. Arrhythmogenic ion-channel remodeling in the heart: heart failure, myocardial infarction, and atrial fibrillation. *Physiological reviews*. 2007;87:425-456. doi: 10.1152/physrev.00014.2006
16. Kucera JP, Rohr S, Rudy Y. Localization of sodium channels in intercalated disks modulates cardiac conduction. *Circulation research*. 2002;91:1176-1182. doi: 10.1161/01.res.0000046237.54156.0a
17. Rohr S. Role of gap junctions in the propagation of the cardiac action potential. *Cardiovascular research*. 2004;62:309-322. doi: 10.1016/j.cardiores.2003.11.035
18. Noutsias M, Fechner H, de Jonge H, Wang X, Dekkers D, Houtsmuller AB, Pauschinger M, Bergelson J, Warraich R, Yacoub M, et al. Human coxsackie-adenovirus receptor is colocalized with integrins alpha(v)beta(3) and alpha(v)beta(5) on the cardiomyocyte

sarcolemma and upregulated in dilated cardiomyopathy: implications for cardiotropic viral infections. *Circulation*. 2001;104:275-280. doi: 10.1161/01.cir.104.3.275
19. Veeraraghavan R, Hoeker GS, Alvarez-Laviada A, Hoagland D, Wan X, King DR, Sanchez-Alonso J, Chen C, Jourdan J, Isom LL, et al. The adhesion function of the sodium channel beta subunit (beta1) contributes to cardiac action potential propagation. *Elife*. 2018;7. doi: 10.7554/eLife.37610
20. George SA, Hoeker G, Calhoun PJ, Entz M, 2nd, Raisch TB, King DR, Khan M, Baker C, Gourdie RG, Smyth JW, et al. Modulating cardiac conduction during metabolic ischemia with perfusate sodium and calcium in guinea pig hearts. *American journal of physiology Heart and circulatory physiology*. 2019;316:H849-H861. doi: 10.1152/ajpheart.00083.2018
21. Agullo-Pascual E, Lin X, Leo-Macias A, Zhang M, Liang FX, Li Z, Pfenniger A, Lubkemeier I, Keegan S, Fenyo D, et al. Super-resolution imaging reveals that loss of the C-terminus of connexin43 limits microtubule plus-end capture and NaV1.5 localization at the intercalated disc. *Cardiovascular research*. 2014;104:371-381. doi: 10.1093/cvr/cvu195
22. Vermij SH, Abriel H, van Veen TA. Refining the molecular organization of the cardiac intercalated disc. *Cardiovascular research*. 2017;113:259-275. doi: 10.1093/cvr/cvw259
23. Palatinus JA, O'Quinn MP, Barker RJ, Harris BS, Jourdan J, Gourdie RG. ZO-1 determines adherens and gap junction localization at intercalated disks. *American journal of physiology Heart and circulatory physiology*. 2011;300:H583-594. doi: 10.1152/ajpheart.00999.2010
24. Chkourko HS, Guerrero-Serna G, Lin X, Darwish N, Pohlmann JR, Cook KE, Martens JR, Rothenberg E, Musa H, Delmar M. Remodeling of mechanical junctions and of microtubule-associated proteins accompany cardiac connexin43 lateralization. *Heart Rhythm*. 2012;9:1133-1140 e1136. doi: 10.1016/j.hrthm.2012.03.003
25. Peters NS, Coromilas J, Severs NJ, Wit AL. Disturbed connexin43 gap junction distribution correlates with the location of reentrant circuits in the epicardial border zone of healing canine infarcts that cause ventricular tachycardia. *Circulation*. 1997;95:988-996.
26. Smyth JW, Hong TT, Gao D, Vogan JM, Jensen BC, Fong TS, Simpson PC, Stainier DY, Chi NC, Shaw RM. Limited forward trafficking of connexin 43 reduces cell-cell coupling in stressed human and mouse myocardium. *The Journal of clinical investigation*. 2010;120:266-279. doi: 10.1172/JCI39740
27. Yajima T, Knowlton KU. Viral myocarditis: from the perspective of the virus. *Circulation*. 2009;119:2615-2624. doi: 10.1161/CIRCULATIONAHA.108.766022
28. Lei M, Xu J, Gao Q, Minobe E, Kameyama M, Hao L. PKA phosphorylation of Cav1.2 channel modulates the interaction of calmodulin with the C terminal tail of the channel. *J Pharmacol Sci*. 2018;137:187-194. doi: 10.1016/j.jphs.2018.05.010
29. Lampe PD, TenBroek EM, Burt JM, Kurata WE, Johnson RG, Lau AF. Phosphorylation of connexin43 on serine368 by protein kinase C regulates gap junctional communication. *The Journal of cell biology*. 2000;149:1503-1512.
30. Ek-Vitorin JF, King TJ, Heyman NS, Lampe PD, Burt JM. Selectivity of connexin 43 channels is regulated through protein kinase C-dependent phosphorylation. *Circulation research*. 2006;98:1498-1505. doi: 10.1161/01.RES.0000227572.45891.2c
31. Kanda VA, Purtell K, Abbott GW. Protein kinase C downregulates I(Ks) by stimulating KCNQ1-KCNE1 potassium channel endocytosis. *Heart Rhythm*. 2011;8:1641-1647. doi: 10.1016/j.hrthm.2011.04.034
32. Jiang M, Xu X, Wang Y, Toyoda F, Liu XS, Zhang M, Robinson RB, Tseng GN. Dynamic partnership between KCNQ1 and KCNE1 and influence on cardiac IKs current amplitude

by KCNE2. *The Journal of biological chemistry*. 2009;284:16452-16462. doi: 10.1074/jbc.M808262200
33. Jongsma HJ, Wilders R. Gap junctions in cardiovascular disease. *Circulation research*. 2000;86:1193-1197.
34. Vozzi C, Dupont E, Coppen SR, Yeh HI, Severs NJ. Chamber-related differences in connexin expression in the human heart. *Journal of molecular and cellular cardiology*. 1999;31:991-1003. doi: 10.1006/jmcc.1999.0937
35. Ablasser A, Schmid-Burgk JL, Hemmerling I, Horvath GL, Schmidt T, Latz E, Hornung V. Cell intrinsic immunity spreads to bystander cells via the intercellular transfer of cGAMP. *Nature*. 2013;503:530-534. doi: 10.1038/nature12640
36. Neijssen J, Herberts C, Drijfhout JW, Reits E, Janssen L, Neefjes J. Cross-presentation by intercellular peptide transfer through gap junctions. *Nature*. 2005;434:83-88. doi: 10.1038/nature03290
37. Patel SJ, King KR, Casali M, Yarmush ML. DNA-triggered innate immune responses are propagated by gap junction communication. *Proceedings of the National Academy of Sciences of the United States of America*. 2009;106:12867-12872. doi: 10.1073/pnas.0809292106
38. Calhoun PJ, Phan AV, Taylor JD, James CC, Padget RL, Zeitz MJ, Smyth JW. Adenovirus targets transcriptional and posttranslational mechanisms to limit gap junction function. *FASEB J*. 2020;34:9694-9712. doi: 10.1096/fj.202000667R
39. Shauer A, Gotsman I, Keren A, Zwas DR, Hellman Y, Durst R, Admon D. Acute viral myocarditis: current concepts in diagnosis and treatment. *Isr Med Assoc J*. 2013;15:180-185.
40. Escher F, Pietsch H, Aleshcheva G, Bock T, Baumeier C, Elsaesser A, Wenzel P, Hamm C, Westenfeld R, Schultheiss M, et al. Detection of viral SARS-CoV-2 genomes and histopathological changes in endomyocardial biopsies. *ESC Heart Fail*. 2020;7:2440-2447. doi: 10.1002/ehf2.12805
41. Garmaroudi FS, Marchant D, Hendry R, Luo H, Yang D, Ye X, Shi J, McManus BM. Coxsackievirus B3 replication and pathogenesis. *Future Microbiol*. 2015;10:629-653. doi: 10.2217/fmb.15.5
42. Knowlton KU. CVB infection and mechanisms of viral cardiomyopathy. *Curr Top Microbiol Immunol*. 2008;323:315-335.
43. Lim BK, Peter AK, Xiong D, Narezkina A, Yung A, Dalton ND, Hwang KK, Yajima T, Chen J, Knowlton KU. Inhibition of Coxsackievirus-associated dystrophin cleavage prevents cardiomyopathy. *The Journal of clinical investigation*. 2013;123:5146-5151. doi: 10.1172/JCI66271
44. Nagy PD, Pogany J. The dependence of viral RNA replication on co-opted host factors. *Nat Rev Microbiol*. 2011;10:137-149. doi: 10.1038/nrmicro2692
45. O'Shea CC. DNA tumor viruses -- the spies who lyse us. *Curr Opin Genet Dev*. 2005;15:18-26. doi: 10.1016/j.gde.2004.12.010
46. Greber UF. Adenoviruses - Infection, pathogenesis and therapy. *FEBS letters*. 2020;594:1818-1827. doi: 10.1002/1873-3468.13849
47. Schneider-Schaulies J. Cellular receptors for viruses: links to tropism and pathogenesis. *J Gen Virol*. 2000;81:1413-1429. doi: 10.1099/0022-1317-81-6-1413
48. Pauschinger M, Bowles NE, Fuentes-Garcia FJ, Pham V, Kuhl U, Schwimmbeck PL, Schultheiss HP, Towbin JA. Detection of adenoviral genome in the myocardium of adult patients with idiopathic left ventricular dysfunction. *Circulation*. 1999;99:1348-1354. doi: 10.1161/01.cir.99.10.1348
49. Treacy A, Carr MJ, Dunford L, Palacios G, Cannon GA, O'Grady A, Moran J, Hassan J, Loy A, Connell J, et al. First report of sudden death due to myocarditis caused by adenovirus serotype 3. *J Clin Microbiol*. 2010;48:642-645. doi: 10.1128/JCM.00815-09

50. Bowles NE, Ni J, Kearney DL, Pauschinger M, Schultheiss HP, McCarthy R, Hare J, Bricker JT, Bowles KR, Towbin JA. Detection of viruses in myocardial tissues by polymerase chain reaction. evidence of adenovirus as a common cause of myocarditis in children and adults. *J Am Coll Cardiol*. 2003;42:466-472.
51. O'Shea CC, Choi S, McCormick F, Stokoe D. Adenovirus overrides cellular checkpoints for protein translation. *Cell Cycle*. 2005;4:883-888.
52. Turner RL, Groitl P, Dobner T, Ornelles DA. Adenovirus replaces mitotic checkpoint controls. *J Virol*. 2015;89:5083-5096. doi: 10.1128/JVI.00213-15
53. Smyth JW, Zhang SS, Sanchez JM, Lamouille S, Vogan JM, Hesketh GG, Hong T, Tomaselli GF, Shaw RM. A 14-3-3 mode-1 binding motif initiates gap junction internalization during acute cardiac ischemia. *Traffic*. 2014;15:684-699. doi: 10.1111/tra.12169
54. Bertzbach LD, Ip WH, Dobner T. Animal Models in Human Adenovirus Research. *Biology (Basel)*. 2021;10. doi: 10.3390/biology10121253
55. McCarthy MK, Procario MC, Twisselmann N, Wilkinson JE, Archambeau AJ, Michele DE, Day SM, Weinberg JB. Proinflammatory effects of interferon gamma in mouse adenovirus 1 myocarditis. *J Virol*. 2015;89:468-479. doi: 10.1128/JVI.02077-14
56. Chandrasekaran A, Adkins LJ, Seltzer HM, Pant K, Tryban ST, Molloy CT, Weinberg JB. Age-Dependent Effects of Immunoproteasome Deficiency on Mouse Adenovirus Type 1 Pathogenesis. *J Virol*. 2019;93. doi: 10.1128/JVI.00569-19
57. Weinberg JB, Stempfle GS, Wilkinson JE, Younger JG, Spindler KR. Acute respiratory infection with mouse adenovirus type 1. *Virology*. 2005;340:245-254. doi: 10.1016/j.virol.2005.06.021
58. Gralinski LE, Ashley SL, Dixon SD, Spindler KR. Mouse adenovirus type 1-induced breakdown of the blood-brain barrier. *J Virol*. 2009;83:9398-9410. doi: 10.1128/JVI.00954-09
59. Klempa B, Kruger DH, Auste B, Stanko M, Krawczyk A, Nickel KF, Uberla K, Stang A. A novel cardiotropic murine adenovirus representing a distinct species of mastadenoviruses. *J Virol*. 2009;83:5749-5759. doi: 10.1128/JVI.02281-08
60. Bieri M, Hendrickx R, Bauer M, Yu B, Jetzer T, Dreier B, Mittl PRE, Sobek J, Pluckthun A, Greber UF, et al. The RGD-binding integrins alphavbeta6 and alphavbeta8 are receptors for mouse adenovirus-1 and -3 infection. *PLoS Pathog*. 2021;17:e1010083. doi: 10.1371/journal.ppat.1010083
61. Burridge PW, Holmstrom A, Wu JC. Chemically Defined Culture and Cardiomyocyte Differentiation of Human Pluripotent Stem Cells. *Curr Protoc Hum Genet*. 2015;87:21 23 21-21 23 15. doi: 10.1002/0471142905.hg2103s87
62. Burridge PW, Matsa E, Shukla P, Lin ZC, Churko JM, Ebert AD, Lan F, Diecke S, Huber B, Mordwinkin NM, et al. Chemically defined generation of human cardiomyocytes. *Nat Methods*. 2014;11:855-860. doi: 10.1038/nmeth.2999
63. Buikema JW, Lee S, Goodyer WR, Maas RG, Chirikian O, Li G, Miao Y, Paige SL, Lee D, Wu H, et al. Wnt Activation and Reduced Cell-Cell Contact Synergistically Induce Massive Expansion of Functional Human iPSC-Derived Cardiomyocytes. *Cell Stem Cell*. 2020;27:50-63 e55. doi: 10.1016/j.stem.2020.06.001
64. Feyen DAM, McKeithan WL, Bruyneel AAN, Spiering S, Hormann L, Ulmer B, Zhang H, Briganti F, Schweizer M, Hegyi B, et al. Metabolic Maturation Media Improve Physiological Function of Human iPSC-Derived Cardiomyocytes. *Cell reports*. 2020;32:107925. doi: 10.1016/j.celrep.2020.107925
65. Green M, Loewenstein PM. Human adenoviruses: propagation, purification, quantification, and storage. *Curr Protoc Microbiol*. 2006;Chapter 14:Unit 14C 11. doi: 10.1002/9780471729259.mc14c01s00

66. O'Connell TD, Rodrigo MC, Simpson PC. Isolation and culture of adult mouse cardiac myocytes. *Methods in molecular biology*. 2007;357:271-296. doi: 10.1385/1-59745-214-9:271
67. Lindsey ML, Escobar GP, Mukherjee R, Goshorn DK, Sheats NJ, Bruce JA, Mains IM, Hendrick JK, Hewett KW, Gourdie RG, et al. Matrix metalloproteinase-7 affects connexin-43 levels, electrical conduction, and survival after myocardial infarction. *Circulation*. 2006;113:2919-2928. doi: 10.1161/CIRCULATIONAHA.106.612960
68. George SA, Sciuto KJ, Lin J, Salama ME, Keener JP, Gourdie RG, Poelzing S. Extracellular sodium and potassium levels modulate cardiac conduction in mice heterozygous null for the Connexin43 gene. *Pflugers Arch*. 2015;467:2287-2297. doi: 10.1007/s00424-015-1698-0
69. King DR, Entz M, 2nd, Blair GA, Crandell I, Hanlon AL, Lin J, Hoeker GS, Poelzing S. The conduction velocity-potassium relationship in the heart is modulated by sodium and calcium. *Pflugers Arch*. 2021;473:557-571. doi: 10.1007/s00424-021-02537-y
70. Smyth JW, Shaw RM. Autoregulation of connexin43 gap junction formation by internally translated isoforms. *Cell reports*. 2013;5:611-618. doi: 10.1016/j.celrep.2013.10.009
71. Zeitz MJ, Calhoun PJ, James CC, Taetzsch T, George KK, Robel S, Valdez G, Smyth JW. Dynamic UTR Usage Regulates Alternative Translation to Modulate Gap Junction Formation during Stress and Aging. *Cell reports*. 2019;27:2737-2747 e2735. doi: 10.1016/j.celrep.2019.04.114
72. Schindelin J, Arganda-Carreras I, Frise E, Kaynig V, Longair M, Pietzsch T, Preibisch S, Rueden C, Saalfeld S, Schmid B, et al. Fiji: an open-source platform for biological-image analysis. *Nat Methods*. 2012;9:676-682. doi: 10.1038/nmeth.2019
73. Walter A, Saric T, Hescheler J, Papadopoulos S. Calcium Imaging in Pluripotent Stem Cell-Derived Cardiac Myocytes. *Methods in molecular biology*. 2016;1353:131-146. doi: 10.1007/7651_2015_267
74. Shaw RM, Rudy Y. Ionic mechanisms of propagation in cardiac tissue. Roles of the sodium and L-type calcium currents during reduced excitability and decreased gap junction coupling. *Circulation research*. 1997;81:727-741.
75. Veeraraghavan R, Lin J, Hoeker GS, Keener JP, Gourdie RG, Poelzing S. Sodium channels in the Cx43 gap junction perinexus may constitute a cardiac ephapse: an experimental and modeling study. *Pflugers Arch*. 2015. doi: 10.1007/s00424-014-1675-z
76. Kirchhoff S, Nelles E, Hagendorff A, Kruger O, Traub O, Willecke K. Reduced cardiac conduction velocity and predisposition to arrhythmias in connexin40-deficient mice. *Curr Biol*. 1998;8:299-302. doi: 10.1016/s0960-9822(98)70114-9
77. Aronis KN, Ali RL, Prakosa A, Ashikaga H, Berger RD, Hakim JB, Liang J, Tandri H, Teng F, Chrispin J, et al. Accurate Conduction Velocity Maps and Their Association With Scar Distribution on Magnetic Resonance Imaging in Patients With Postinfarction Ventricular Tachycardias. *Circ Arrhythm Electrophysiol*. 2020;13:e007792. doi: 10.1161/CIRCEP.119.007792
78. Akar FG, Nass RD, Hahn S, Cingolani E, Shah M, Hesketh GG, DiSilvestre D, Tunin RS, Kass DA, Tomaselli GF. Dynamic changes in conduction velocity and gap junction properties during development of pacing-induced heart failure. *American journal of physiology Heart and circulatory physiology*. 2007;293:H1223-1230. doi: 10.1152/ajpheart.00079.2007
79. Poelzing S, Rosenbaum DS. Altered connexin43 expression produces arrhythmia substrate in heart failure. *American journal of physiology Heart and circulatory physiology*. 2004;287:H1762-1770. doi: 10.1152/ajpheart.00346.2004
80. Akar FG, Spragg DD, Tunin RS, Kass DA, Tomaselli GF. Mechanisms underlying conduction slowing and arrhythmogenesis in nonischemic dilated cardiomyopathy. *Circulation research*. 2004;95:717-725. doi: 10.1161/01.RES.0000144125.61927.1c

81. Smyth JW, Vogan JM, Buch PJ, Zhang SS, Fong TS, Hong TT, Shaw RM. Actin cytoskeleton rest stops regulate anterograde traffic of connexin 43 vesicles to the plasma membrane. *Circulation research*. 2012;110:978-989. doi: 10.1161/CIRCRESAHA.111.257964
82. Pollack A, Kontorovich AR, Fuster V, Dec GW. Viral myocarditis--diagnosis, treatment options, and current controversies. *Nat Rev Cardiol*. 2015;12:670-680. doi: 10.1038/nrcardio.2015.108
83. Martens CR, Accornero F. Viruses in the Heart: Direct and Indirect Routes to Myocarditis and Heart Failure. *Viruses*. 2021;13. doi: 10.3390/v13101924
84. Kearney MT, Cotton JM, Richardson PJ, Shah AM. Viral myocarditis and dilated cardiomyopathy: mechanisms, manifestations, and management. *Postgrad Med J*. 2001;77:4-10. doi: 10.1136/pmj.77.903.4
85. Kuhl U, Pauschinger M, Noutsias M, Seeberg B, Bock T, Lassner D, Poller W, Kandolf R, Schultheiss HP. High prevalence of viral genomes and multiple viral infections in the myocardium of adults with "idiopathic" left ventricular dysfunction. *Circulation*. 2005;111:887-893. doi: 10.1161/01.CIR.0000155616.07901.35
86. Spurgeon ME, Ornelles DA. The adenovirus E1B 55-kilodalton and E4 open reading frame 6 proteins limit phosphorylation of eIF2alpha during the late phase of infection. *J Virol*. 2009;83:9970-9982. doi: 10.1128/JVI.01113-09
87. Yueh A, Schneider RJ. Selective translation initiation by ribosome jumping in adenovirus-infected and heat-shocked cells. *Genes Dev*. 1996;10:1557-1567. doi: 10.1101/gad.10.12.1557
88. Huke S, Venkataraman R, Faggioni M, Bennuri S, Hwang HS, Baudenbacher F, Knollmann BC. Focal energy deprivation underlies arrhythmia susceptibility in mice with calcium-sensitized myofilaments. *Circulation research*. 2013;112:1334-1344. doi: 10.1161/CIRCRESAHA.113.301055
89. Delmar M, Michaels DC, Johnson T, Jalife J. Effects of increasing intercellular resistance on transverse and longitudinal propagation in sheep epicardial muscle. *Circulation research*. 1987;60:780-785. doi: 10.1161/01.res.60.5.780
90. Dhein S, Krusemann K, Schaefer T. Effects of the gap junction uncoupler palmitoleic acid on the activation and repolarization wavefronts in isolated rabbit hearts. *Br J Pharmacol*. 1999;128:1375-1384. doi: 10.1038/sj.bjp.0702902
91. Fast VG, Darrow BJ, Saffitz JE, Kleber AG. Anisotropic activation spread in heart cell monolayers assessed by high-resolution optical mapping. Role of tissue discontinuities. *Circulation research*. 1996;79:115-127. doi: 10.1161/01.res.79.1.115
92. Toure A, Cabo C. Effect of cell geometry on conduction velocity in a subcellular model of myocardium. *IEEE Trans Biomed Eng*. 2010;57:2107-2114. doi: 10.1109/TBME.2010.2050064
93. Hubbard ML, Ying W, Henriquez CS. Effect of gap junction distribution on impulse propagation in a monolayer of myocytes: a model study. *Europace*. 2007;9 Suppl 6:vi20-28. doi: 10.1093/europace/eum203
94. Danave IR, Tiffany-Castiglioni E, Zenger E, Barhoumi R, Burghardt RC, Collisson EW. Feline immunodeficiency virus decreases cell-cell communication and mitochondrial membrane potential. *J Virol*. 1994;68:6745-6750. doi: 10.1128/JVI.68.10.6745-6750.1994
95. Faccini AM, Cairney M, Ashrafi GH, Finbow ME, Campo MS, Pitts JD. The bovine papillomavirus type 4 E8 protein binds to ductin and causes loss of gap junctional intercellular communication in primary fibroblasts. *J Virol*. 1996;70:9041-9045. doi: 10.1128/JVI.70.12.9041-9045.1996

96. Knabb MT, Danielsen CA, McShane-Kay K, Mbuy GK, Woodruff RI. Herpes simplex virus-type 2 infectivity and agents that block gap junctional intercellular communication. *Virus Res*. 2007;124:212-219. doi: 10.1016/j.virusres.2006.11.006
97. Crow DS, Beyer EC, Paul DL, Kobe SS, Lau AF. Phosphorylation of connexin43 gap junction protein in uninfected and Rous sarcoma virus-transformed mammalian fibroblasts. *Mol Cell Biol*. 1990;10:1754-1763. doi: 10.1128/mcb.10.4.1754-1763.1990
98. Sun P, Dong L, MacDonald AI, Akbari S, Edward M, Hodgins MB, Johnstone SR, Graham SV. HPV16 E6 Controls the Gap Junction Protein Cx43 in Cervical Tumour Cells. *Viruses*. 2015;7:5243-5256. doi: 10.3390/v7102871
99. Chang LS, Shenk T. The adenovirus DNA-binding protein stimulates the rate of transcription directed by adenovirus and adeno-associated virus promoters. *J Virol*. 1990;64:2103-2109. doi: 10.1128/JVI.64.5.2103-2109.1990
100. Logan J, Shenk T. Adenovirus tripartite leader sequence enhances translation of mRNAs late after infection. *Proceedings of the National Academy of Sciences of the United States of America*. 1984;81:3655-3659. doi: 10.1073/pnas.81.12.3655
101. Blazquez AB, Vazquez-Calvo A, Martin-Acebes MA, Saiz JC. Pharmacological Inhibition of Protein Kinase C Reduces West Nile Virus Replication. *Viruses*. 2018;10. doi: 10.3390/v10020091
102. Blazquez AB, Saiz JC. Potential for Protein Kinase Pharmacological Regulation in Flaviviridae Infections. *International journal of molecular sciences*. 2020;21. doi: 10.3390/ijms21249524
103. Nakano MY, Boucke K, Suomalainen M, Stidwill RP, Greber UF. The first step of adenovirus type 2 disassembly occurs at the cell surface, independently of endocytosis and escape to the cytosol. *J Virol*. 2000;74:7085-7095. doi: 10.1128/jvi.74.15.7085-7095.2000
104. Yousuf MA, Lee JS, Zhou X, Ramke M, Lee JY, Chodosh J, Rajaiya J. Protein Kinase C Signaling in Adenoviral Infection. *Biochemistry*. 2016;55:5938-5946. doi: 10.1021/acs.biochem.6b00858
105. Castagna M, Takai Y, Kaibuchi K, Sano K, Kikkawa U, Nishizuka Y. Direct activation of calcium-activated, phospholipid-dependent protein kinase by tumor-promoting phorbol esters. *The Journal of biological chemistry*. 1982;257:7847-7851.
106. Black AR, Black JD. Protein kinase C signaling and cell cycle regulation. *Front Immunol*. 2012;3:423. doi: 10.3389/fimmu.2012.00423
107. Soh JW, Weinstein IB. Roles of specific isoforms of protein kinase C in the transcriptional control of cyclin D1 and related genes. *The Journal of biological chemistry*. 2003;278:34709-34716. doi: 10.1074/jbc.M302016200
108. Grand RJ, Ibrahim AP, Taylor AM, Milner AE, Gregory CD, Gallimore PH, Turnell AS. Human cells arrest in S phase in response to adenovirus 12 E1A. *Virology*. 1998;244:330-342. doi: 10.1006/viro.1998.9102
109. Ben-Israel H, Kleinberger T. Adenovirus and cell cycle control. *Front Biosci*. 2002;7:d1369-1395. doi: 10.2741/ben
110. Zheng X, Rao XM, Gomez-Gutierrez JG, Hao H, McMasters KM, Zhou HS. Adenovirus E1B55K region is required to enhance cyclin E expression for efficient viral DNA replication. *J Virol*. 2008;82:3415-3427. doi: 10.1128/JVI.01708-07
111. Pasumarthi KB, Field LJ. Cardiomyocyte cell cycle regulation. *Circulation research*. 2002;90:1044-1054. doi: 10.1161/01.res.0000020201.44772.67
112. Kaab S, Nuss HB, Chiamvimonvat N, O'Rourke B, Pak PH, Kass DA, Marban E, Tomaselli GF. Ionic mechanism of action potential prolongation in ventricular myocytes from dogs with pacing-induced heart failure. *Circulation research*. 1996;78:262-273. doi: 10.1161/01.res.78.2.262

113. Plaster NM, Tawil R, Tristani-Firouzi M, Canun S, Bendahhou S, Tsunoda A, Donaldson MR, Iannaccone ST, Brunt E, Barohn R, et al. Mutations in Kir2.1 cause the developmental and episodic electrical phenotypes of Andersen's syndrome. *Cell*. 2001;105:511-519. doi: 10.1016/s0092-8674(01)00342-7
114. Tristani-Firouzi M, Jensen JL, Donaldson MR, Sansone V, Meola G, Hahn A, Bendahhou S, Kwiecinski H, Fidzianska A, Plaster N, et al. Functional and clinical characterization of KCNJ2 mutations associated with LQT7 (Andersen syndrome). *The Journal of clinical investigation*. 2002;110:381-388. doi: 10.1172/JCI15183
115. Tsuboi M, Antzelevitch C. Cellular basis for electrocardiographic and arrhythmic manifestations of Andersen-Tawil syndrome (LQT7). *Heart Rhythm*. 2006;3:328-335. doi: 10.1016/j.hrthm.2005.11.026
116. Reilly L, Alvarado FJ, Lang D, Abozeid S, Van Ert H, Spellman C, Warden J, Makielski JC, Glukhov AV, Eckhardt LL. Genetic Loss of IK1 Causes Adrenergic-Induced Phase 3 Early Afterdepolariz ations and Polymorphic and Bidirectional Ventricular Tachycardia. *Circ Arrhythm Electrophysiol*. 2020;13:e008638. doi: 10.1161/CIRCEP.120.008638
117. Sanguinetti MC, Curran ME, Zou A, Shen J, Spector PS, Atkinson DL, Keating MT. Coassembly of K(V)LQT1 and minK (IsK) proteins to form cardiac I(Ks) potassium channel. *Nature*. 1996;384:80-83. doi: 10.1038/384080a0
118. Sanguinetti MC. Dysfunction of delayed rectifier potassium channels in an inherited cardiac arrhythmia. *Annals of the New York Academy of Sciences*. 1999;868:406-413. doi: 10.1111/j.1749-6632.1999.tb11302.x
119. Aromolaran AS, Subramanyam P, Chang DD, Kobertz WR, Colecraft HM. LQT1 mutations in KCNQ1 C-terminus assembly domain suppress IKs using different mechanisms. *Cardiovascular research*. 2014;104:501-511. doi: 10.1093/cvr/cvu231
120. Eleftherianos I, Won S, Chtarbanova S, Squiban B, Ocorr K, Bodmer R, Beutler B, Hoffmann JA, Imler JL. ATP-sensitive potassium channel (K(ATP))-dependent regulation of cardiotropic viral infections. *Proceedings of the National Academy of Sciences of the United States of America*. 2011;108:12024-12029. doi: 10.1073/pnas.1108926108
121. Croker B, Crozat K, Berger M, Xia Y, Sovath S, Schaffer L, Eleftherianos I, Imler JL, Beutler B. ATP-sensitive potassium channels mediate survival during infection in mammals and insects. *Nat Genet*. 2007;39:1453-1460. doi: 10.1038/ng.2007.25
122. Iwata M, Komori S, Unno T, Minamoto N, Ohashi H. Modification of membrane currents in mouse neuroblastoma cells following infection with rabies virus. *Br J Pharmacol*. 1999;126:1691-1698. doi: 10.1038/sj.bjp.0702473
123. Cahalan MD, Chandy KG. The functional network of ion channels in T lymphocytes. *Immunol Rev*. 2009;231:59-87. doi: 10.1111/j.1600-065X.2009.00816.x
124. Cotton CU. Basolateral potassium channels and epithelial ion transport. *Am J Respir Cell Mol Biol*. 2000;23:270-272. doi: 10.1165/ajrcmb.23.3.f198
125. Villalonga N, David M, Bielanska J, Vicente R, Comes N, Valenzuela C, Felipe A. Immunomodulation of voltage-dependent K+ channels in macrophages: molecular and biophysical consequences. *J Gen Physiol*. 2010;135:135-147. doi: 10.1085/jgp.200910334
126. Surawicz B. Role of potassium channels in cycle length dependent regulation of action potential duration in mammalian cardiac Purkinje and ventricular muscle fibres. *Cardiovascular research*. 1992;26:1021-1029. doi: 10.1093/cvr/26.11.1021
127. Solan JL, Marquez-Rosado L, Sorgen PL, Thornton PJ, Gafken PR, Lampe PD. Phosphorylation at S365 is a gatekeeper event that changes the structure of Cx43 and prevents down-regulation by PKC. *The Journal of cell biology*. 2007;179:1301-1309. doi: 10.1083/jcb.200707060
128. Karle CA, Zitron E, Zhang W, Wendt-Nordahl G, Kathofer S, Thomas D, Gut B, Scholz E, Vahl CF, Katus HA, et al. Human cardiac inwardly-rectifying K+ channel Kir(2.1b) is

inhibited by direct protein kinase C-dependent regulation in human isolated cardiomyocytes and in an expression system. *Circulation*. 2002;106:1493-1499. doi: 10.1161/01.cir.0000029747.53262.5c
129. Alvi F, Idkowiak-Baldys J, Baldys A, Raymond JR, Hannun YA. Regulation of membrane trafficking and endocytosis by protein kinase C: emerging role of the pericentrion, a novel protein kinase C-dependent subset of recycling endosomes. *Cell Mol Life Sci*. 2007;64:263-270. doi: 10.1007/s00018-006-6363-5
130. Mondal A, Dawson AR, Potts GK, Freiberger EC, Baker SF, Moser LA, Bernard KA, Coon JJ, Mehle A. Influenza virus recruits host protein kinase C to control assembly and activity of its replication machinery. *Elife*. 2017;6. doi: 10.7554/eLife.26910
131. Sieczkarski SB, Brown HA, Whittaker GR. Role of protein kinase C betaII in influenza virus entry via late endosomes. *J Virol*. 2003;77:460-469. doi: 10.1128/jvi.77.1.460-469.2003
132. San-Juan-Vergara H, Peeples ME, Lockey RF, Mohapatra SS. Protein kinase C-alpha activity is required for respiratory syncytial virus fusion to human bronchial epithelial cells. *J Virol*. 2004;78:13717-13726. doi: 10.1128/JVI.78.24.13717-13726.2004
133. Bergelson JM, Cunningham JA, Droguett G, Kurt-Jones EA, Krithivas A, Hong JS, Horwitz MS, Crowell RL, Finberg RW. Isolation of a common receptor for Coxsackie B viruses and adenoviruses 2 and 5. *Science*. 1997;275:1320-1323.
134. Tomko RP, Xu R, Philipson L. HCAR and MCAR: the human and mouse cellular receptors for subgroup C adenoviruses and group B coxsackieviruses. *Proceedings of the National Academy of Sciences of the United States of America*. 1997;94:3352-3356. doi: 10.1073/pnas.94.7.3352
135. Lyle C, McCormick F. Integrin alphavbeta5 is a primary receptor for adenovirus in CAR-negative cells. *Virol J*. 2010;7:148. doi: 10.1186/1743-422X-7-148
136. Lim BK, Xiong D, Dorner A, Youn TJ, Yung A, Liu TI, Gu Y, Dalton ND, Wright AT, Evans SM, et al. Coxsackievirus and adenovirus receptor (CAR) mediates atrioventricular-node function and connexin 45 localization in the murine heart. *The Journal of clinical investigation*. 2008;118:2758-2770. doi: 10.1172/JCI34777
137. Dorner AA, Wegmann F, Butz S, Wolburg-Buchholz K, Wolburg H, Mack A, Nasdala I, August B, Westermann J, Rathjen FG, et al. Coxsackievirus-adenovirus receptor (CAR) is essential for early embryonic cardiac development. *Journal of cell science*. 2005;118:3509-3521. doi: 10.1242/jcs.02476
138. Lisewski U, Shi Y, Wrackmeyer U, Fischer R, Chen C, Schirdewan A, Juttner R, Rathjen F, Poller W, Radke MH, et al. The tight junction protein CAR regulates cardiac conduction and cell-cell communication. *J Exp Med*. 2008;205:2369-2379. doi: 10.1084/jem.20080897
139. Ortiz-Zapater E, Santis G, Parsons M. CAR: A key regulator of adhesion and inflammation. *Int J Biochem Cell Biol*. 2017;89:1-5. doi: 10.1016/j.biocel.2017.05.025
140. Guglielmi KM, Johnson EM, Stehle T, Dermody TS. Attachment and cell entry of mammalian orthoreovirus. *Curr Top Microbiol Immunol*. 2006;309:1-38. doi: 10.1007/3-540-30773-7_1
141. Baty CJ, Sherry B. Cytopathogenic effect in cardiac myocytes but not in cardiac fibroblasts is correlated with reovirus-induced acute myocarditis. *J Virol*. 1993;67:6295-6298. doi: 10.1128/JVI.67.10.6295-6298.1993
142. Sherry B, Baty CJ, Blum MA. Reovirus-induced acute myocarditis in mice correlates with viral RNA synthesis rather than generation of infectious virus in cardiac myocytes. *J Virol*. 1996;70:6709-6715. doi: 10.1128/JVI.70.10.6709-6715.1996
143. McCarthy MK, Malitz DH, Molloy CT, Procario MC, Greiner KE, Zhang L, Wang P, Day SM, Powell SR, Weinberg JB. Interferon-dependent immunoproteasome activity during

mouse adenovirus type 1 infection. *Virology*. 2016;498:57-68. doi: 10.1016/j.virol.2016.08.009

144. Hemmi S, Spindler KR. Murine adenoviruses: tools for studying adenovirus pathogenesis in a natural host. *FEBS letters*. 2019;593:3649-3659. doi: 10.1002/1873-3468.13699

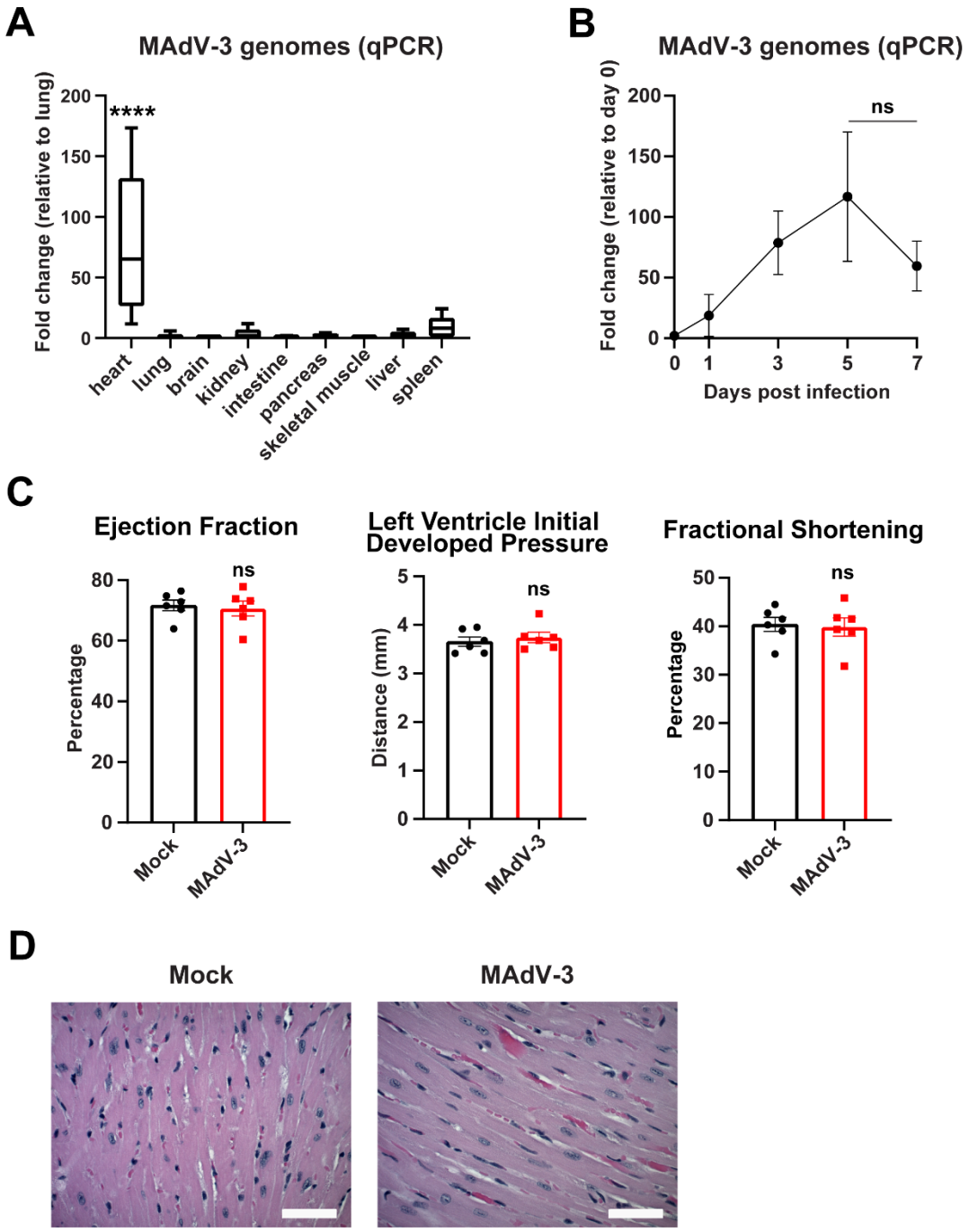

Figure 1. Mouse adenovirus type-3 is cardiotropic and does not invoke an appreciable immune response or cardiomyopathy during acute infection. Mice were infected intranasally with $5x10^5$ i.u. MAdV-3 or saline (mock) and tissues were harvested 7 d.p.i. **A)** Using quantitative PCR, MAdV-3 viral genomes were measured across major organs and compared to organ lung tissue as a reference (n=12). **B)** In heart tissue alone, MAdV-3 viral genomes were quantified by qPCR over a 7 day time course (n=3). **C)** Cardiac function was measure by echocardiography on lightly anesthetized mock- and MAdV-3-infected mice (n=6). **D)** Histopathology by H&E staining on paraffin embedded cardiac sections (scale bar: 50 µm). *p ≤ 0.05, **p ≤ 0 .01, ***p ≤ 0.001, ****p ≤ 0.0001, one-way ANOVA (**A**, **B**), Student's t-test (**C**). Data are represented as mean ± SEM.

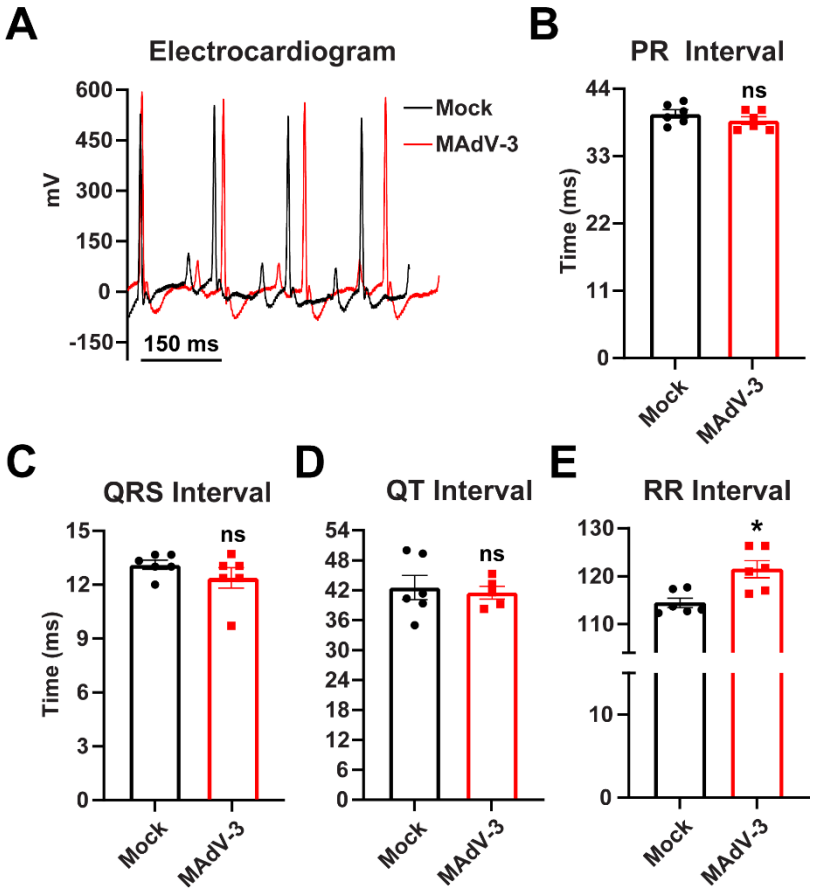

Figure 2. Acute cardiac adenoviral infection slows heart rate but does not alter ECG morphology. *In vivo* electrocardiography was performed 7 d.p.i. in mock- or MAdV-3-infected mice. **A)** Representative *in vivo* electrocardiography measurements from lightly anesthetized mock- and MAdv-3-infected mice using paw pad electrodes. **B-E)** Quantification of PR, QRS, QT, and RR intervals from **A**. *$p \leq 0.05$, student's t-test (n=6).

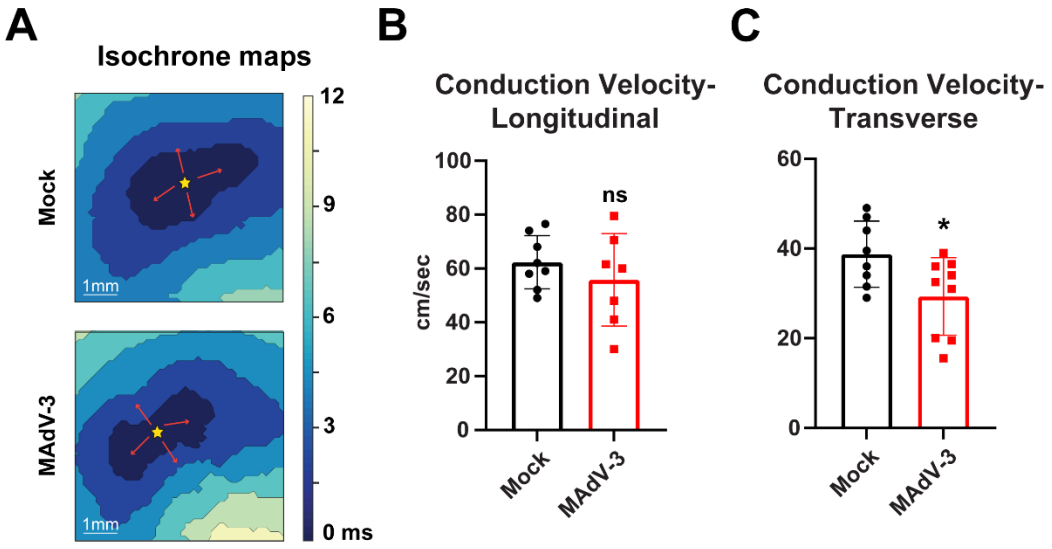

Figure 3. Acute cardiac adenoviral infection results in reduced ventricular conduction velocity. *Ex vivo* optical mapping was performed on Langendorff-perfused hearts 7 d.p.i. from mock- or MAdV-3-infected mice. **A)** Example isochrones maps paced at a cycle length of 150 ms with 1 ms pulse duration. **B, C)** Conduction velocity in longitudinal (CVL)and transverse (CVT) directions (CV_T) was quantified (n=8,9). *p≤0.05, student's t-test. Data are represented as mean ± SEM.

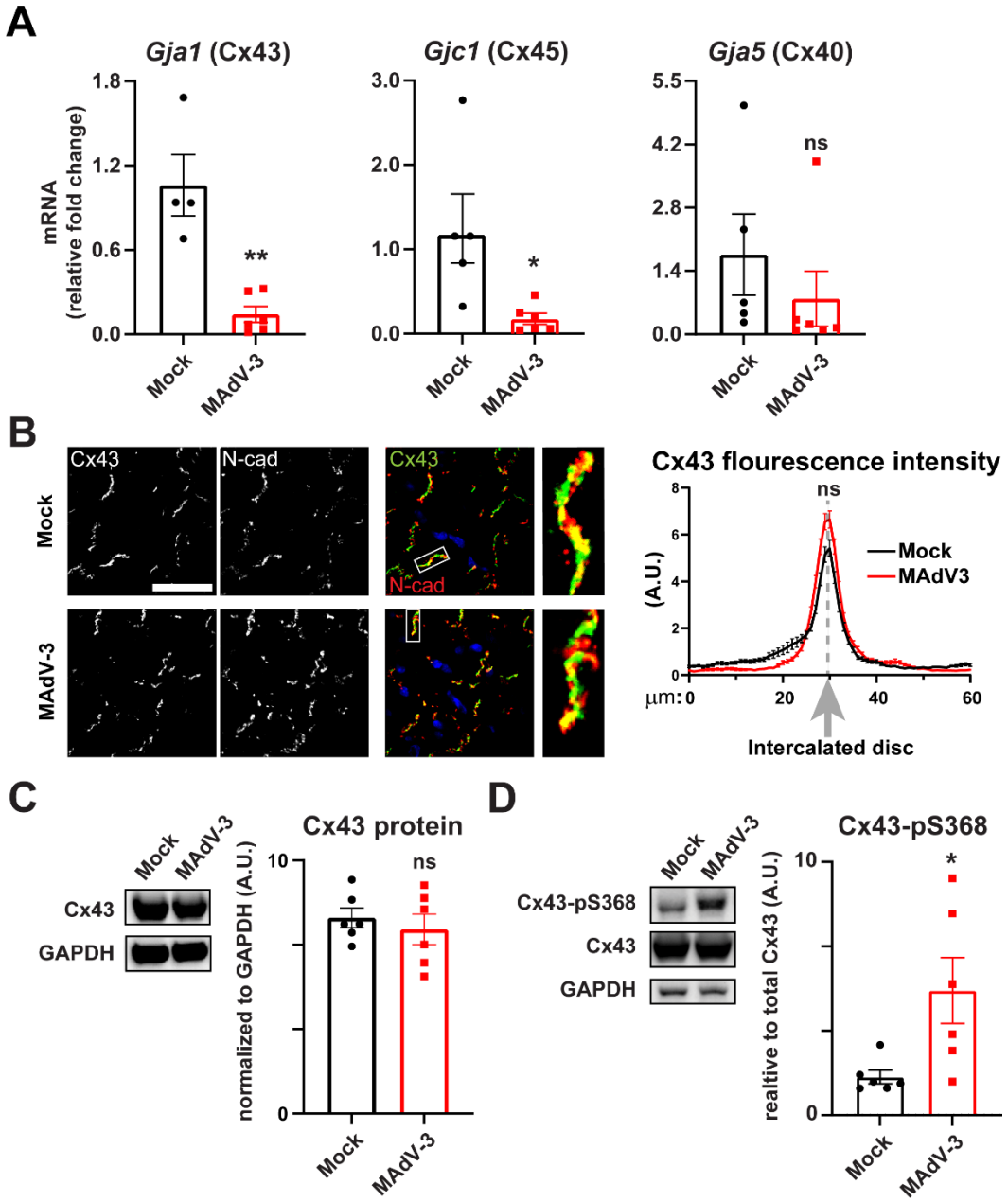

Figure 4. Acute adenovirus infection alters connexin gene expression and elicits increased connexin43 Ser368 phosphorylation. Mice were infected intranasally with $5x10^5$ i.u. MAdV-3 or saline (mock) and cardiac tissue was harvested 7 d.p.i. for analyses. **A)** RT-qPCR of heart tissue mRNA for major cardiac gap junction genes *Gja1*, *Gjc1*, and *Gja5*. **B)** Confocal immunofluorescence microscopy from cryosections to detect Cx43 (green) and N-cadherin (red), with quantification of fluorescent intensity line scans across intercalated discs on right (scale bar: 50 µm). **C)** Western blotting of cardiac ventricle tissue probed for Cx43, with GAPDH as loading control to normalize quantitation on right. **D)** Western blotting of cardiac ventricle tissue probed for phospho-Cx43 Ser368 with quantification normalized to total Cx43 on right. *p ≤ 0.05, **p ≤ 0.01, student's t-test. Data are represented as mean ± SEM.

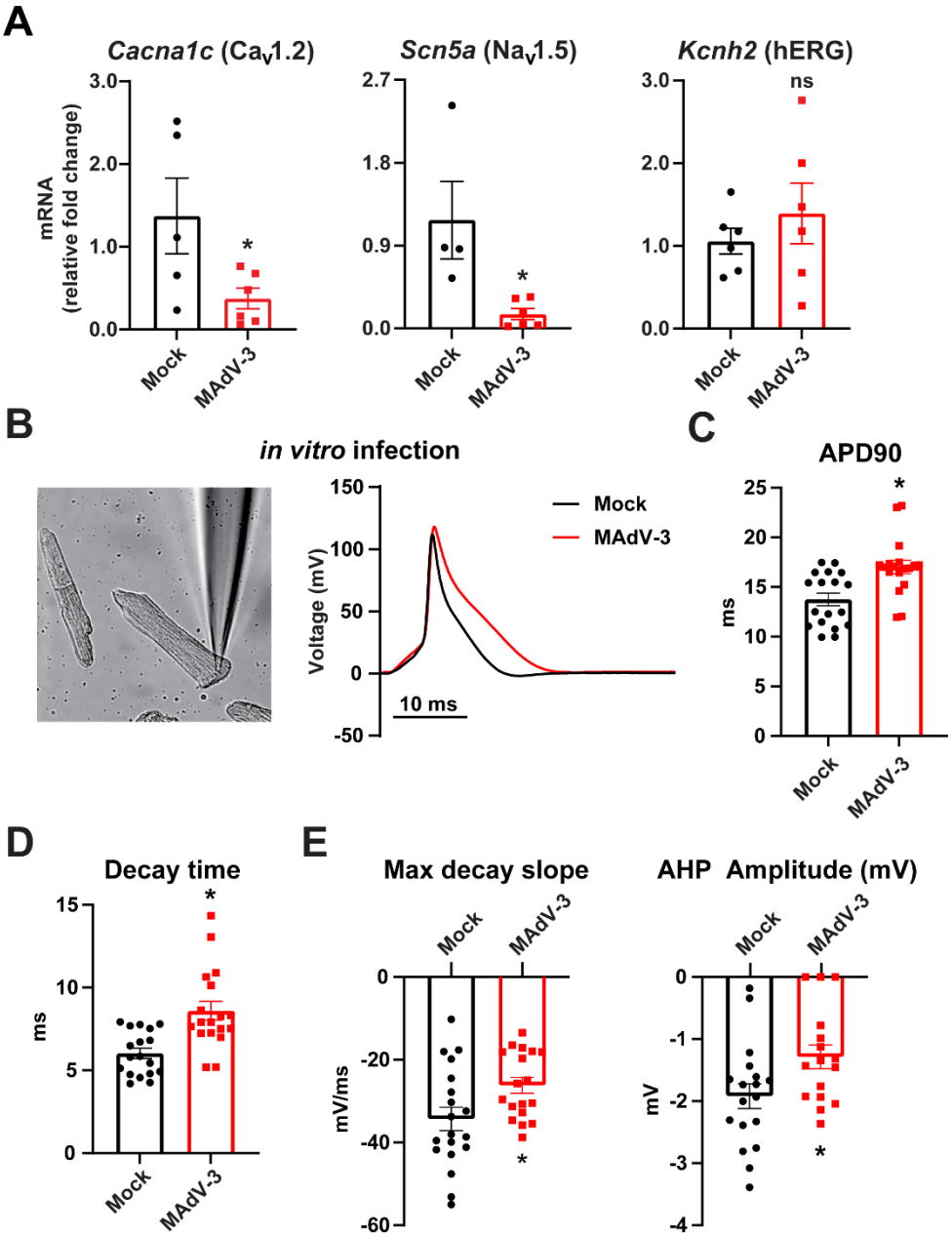

Figure 5. Acute mouse adenovirus infection alters ion channel gene expression *in vivo and* prolongs ventricular cardiomyocyte action potential duration *in vitro*. Mice were infected intranasally with $5x10^5$ i.u. MAdV-3 or saline (mock) and cardiac tissue was harvested 7 d.p.i. for analyses or isolated ACMs were either infected with MAdV-3 at an MOI 10 or not and harvested 24 h.p.i. *in vitro*. **A)** RT-qPCR of heart tissue mRNA for major cardiac ion channel genes *Cacna1c*, *Scn5a*, and *Kcnh2*. **B)** Representative image of ACMs used for patch clamp experiments with representative action potential traces recorded from uninfected (black) and MAdV-3-infected (red) cells. **C)** Action potential duration at 90% repolarization was recorded in uninfected and MAdV-3-infected ACMs (n=18). **D)** Decay time was recorded in uninfected and MAdV-3-infected ACMs (n=18). **E)** Max decay slope and afterpolarization amplitude was recorded in uninfected and MAdV-3-infected ACMs (n=18). *$p \leq 0.05$, **$p \leq 0.01$, Mann-Whitney U test **(C)** or student's t-test **(D,E)**. Data are represented as mean ± SEM.

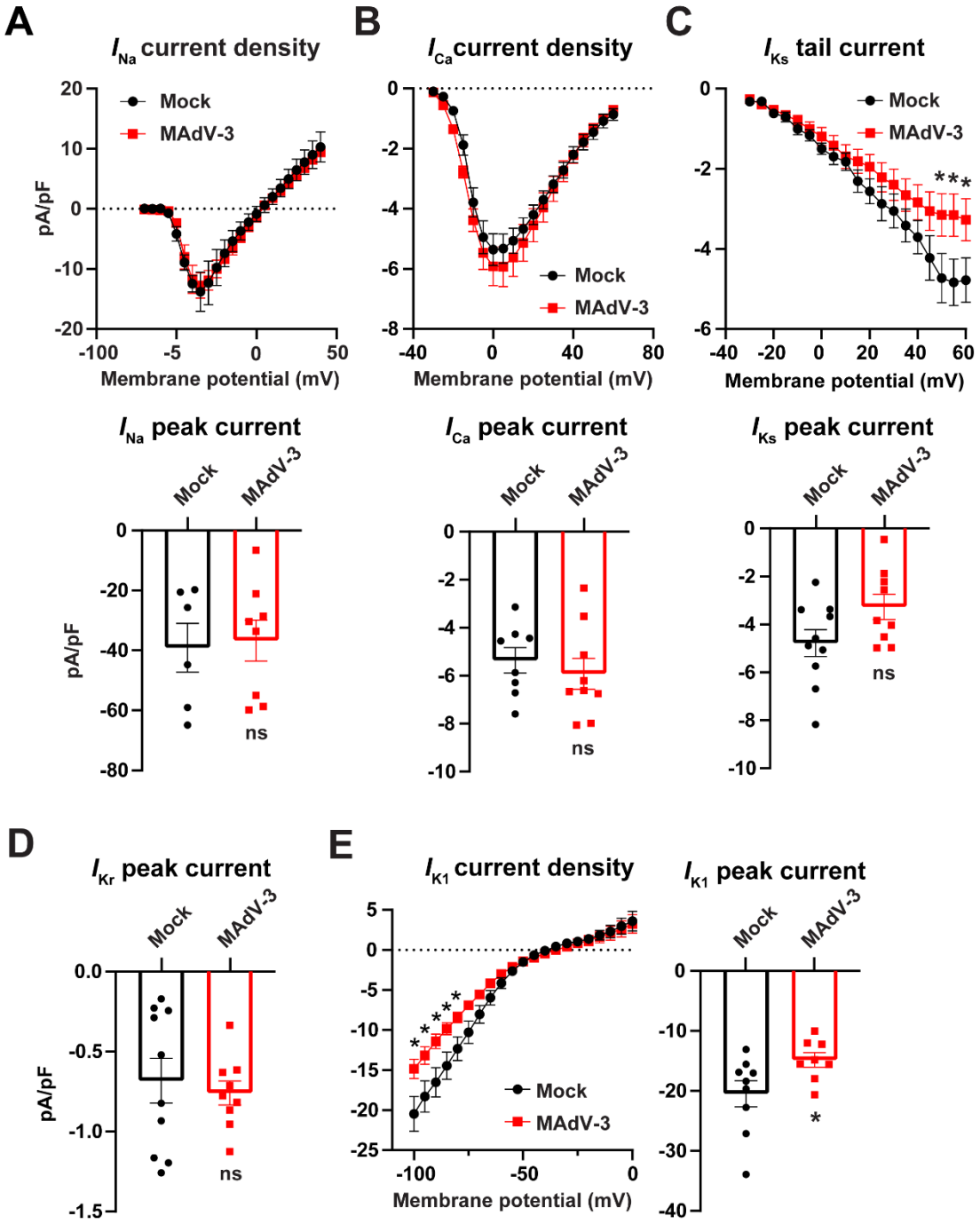

Figure 6. Acute mouse adenovirus infection decreases I_{K1} and I_{KS} current density in isolated adult mouse cardiomyocytes. Isolated ACMs were infected with MAdV-3 at an MOI 10 and analyzed 24 h.p.i. **A)** Current density measured isolated ACMs at 24 h.p.i. for I_{Na}, n=6,8. **B)** Current density measured isolated ACMs at 24 h.p.i. for I_{Ca}, n=8,9 **C)** Current density measured isolated ACMs at 24 h.p.i. for I_{Ks},n=10, 9 D) Current density measured isolated ACMs at 24 h.p.i. for I_{Kr}, n=10,9 E) Current density measured isolated ACMs at 24 h.p.i. for I_{K1}, n=9,8. *p ≤ 0.05, student's t-test. Data are represented as mean ± SEM.

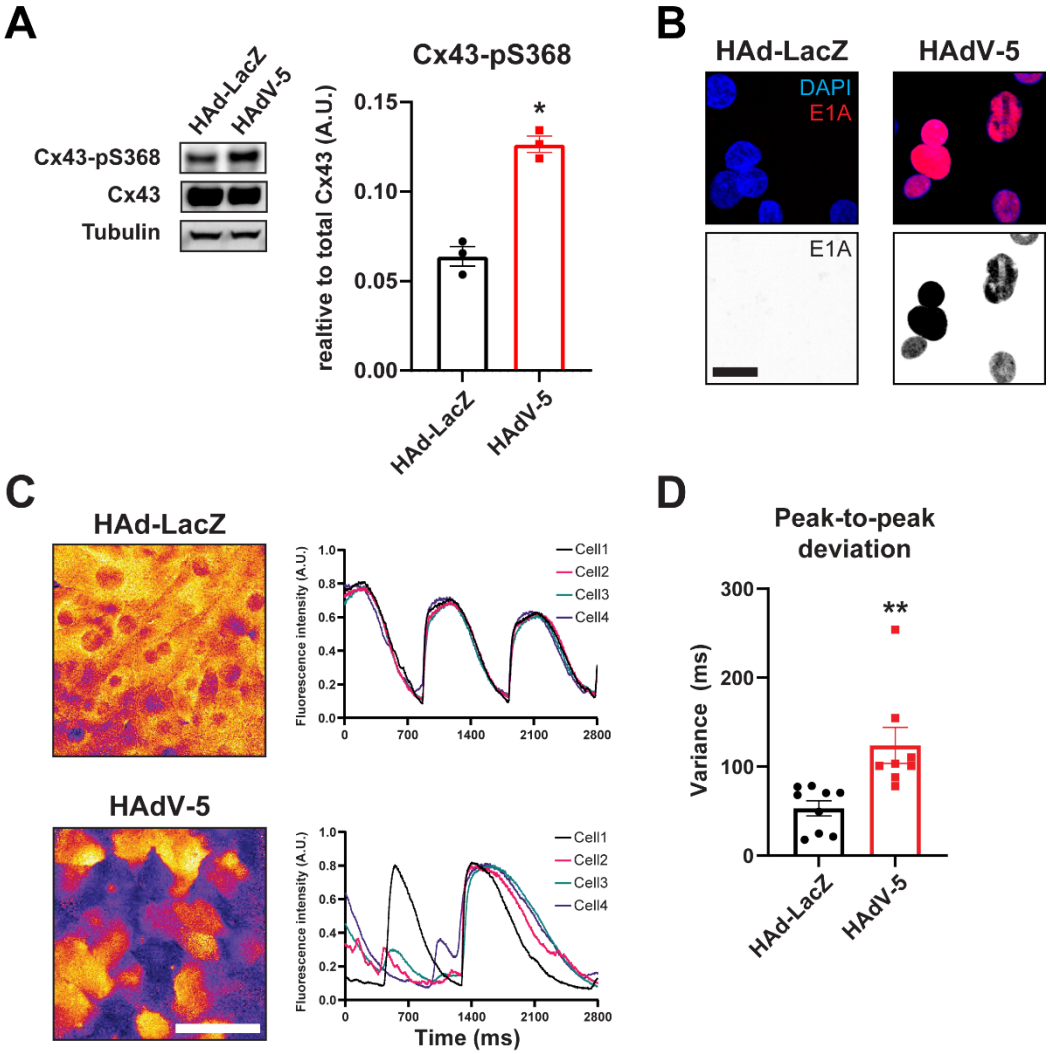

Figure 7. Human Adenovirus Type-5 infection increases Cx43-Ser368 phosphorylation and uncouples HiPSC-derived cardiomyocytes.
HiPSC-CMs were infected with HAdV-LacZ or HAdV-5 at an MOI 10 and harvested 24 h.p.i. **A)** Western blotting of cells probed for phospho-Cx43 Ser368 with quantification normalized to total Cx43 on right (n=3). **B)** Confocal immunofluorescence microscopy from fixed HiPSC-CMs to detect nuclei (blue) and Human Adenoviral protein E1A (red) (scale bar: 25 µm). **C)** Live-cell confocal microscopy 24 h.p.i. using Fluo-4 AM to measure Ca^{2+} transients and quantification of fluorescence signaling over time in one field of view (scale bar: 25 µm). **D)** Average peak-to-peak fluorescence intensity variance measured per cell over time (n=9). *p ≤ 0.05, **p 0.01, student's t-test. Data are represented as mean ± SEM.

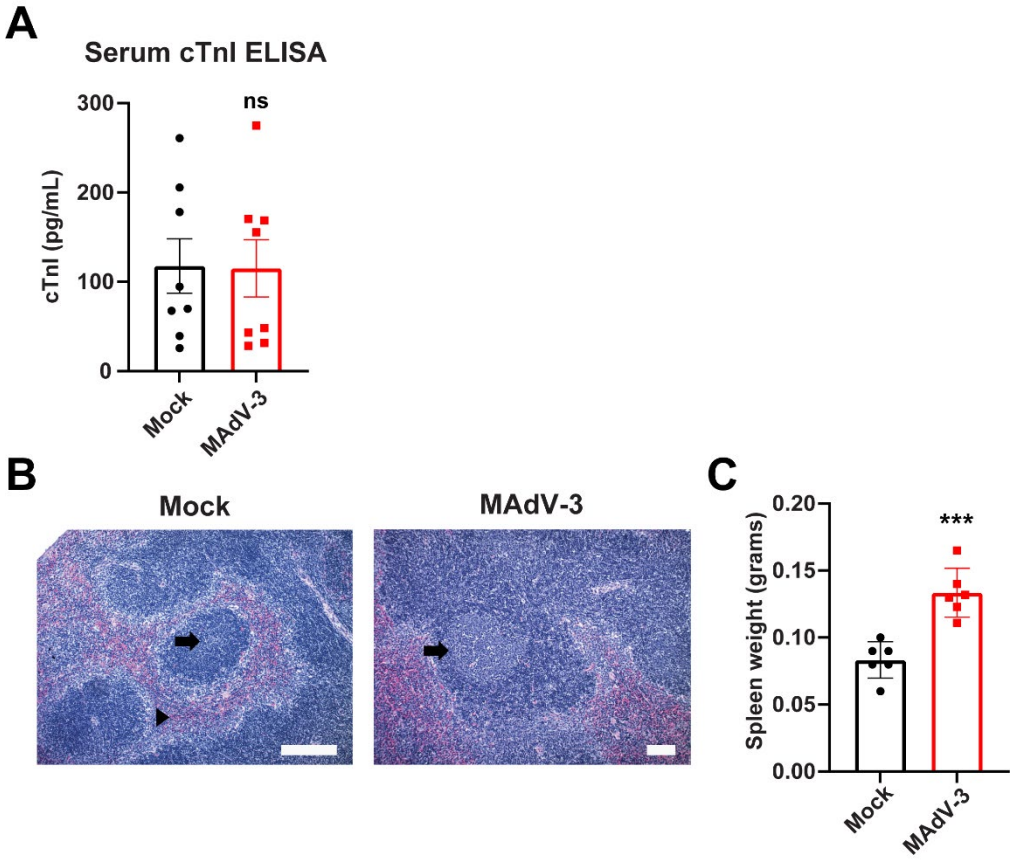

Supplemental Figure 1. Acute MAdV-3 infection does not induce increased cardiac troponin serum levels but does increase spleen weight. Mice were infected intranasally with $5x10^5$ i.u. MAdV-3 or saline (mock) and spleen tissue or serum was harvested 7 d.p.i. for analyses. **A)** Cardiac troponin I ELISA from circulating blood serum of mock or MAdV-3 infected mice was quantified (n=8). **B)** Histopathology by H&E staining on paraffin embedded spleen sections (scale bar: 100µm). **C)** Gross spleen weights (n=6). ***$p \leq 0.001$, student's t-test. Data are represented as mean ± SEM.

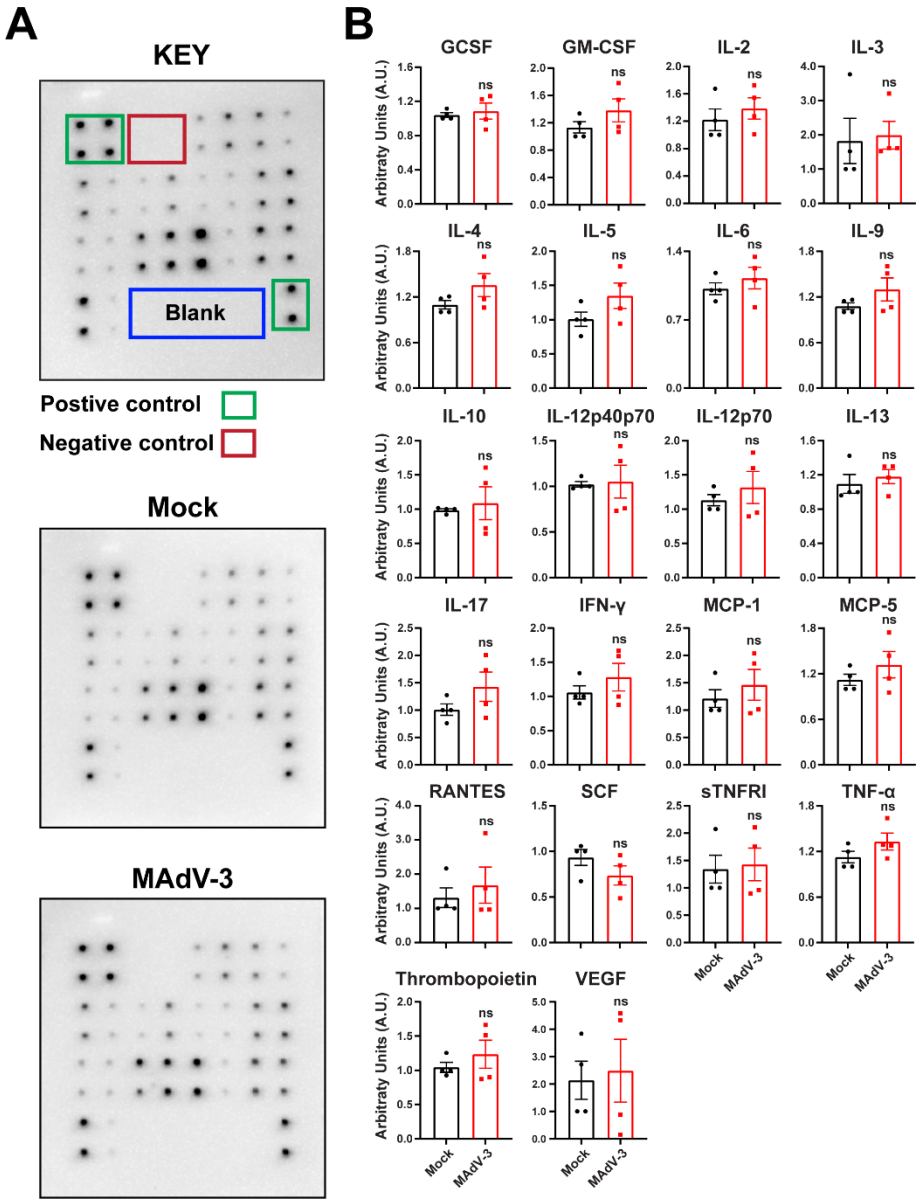

Supplemental Figure 2. Acute MAdV-3 infection does not a detectable cytokine response in the heart 7 days post infection. Mice were infected intranasally with $5x10^5$ i.u. MAdV-3 or saline (mock) and cardiac tissue was harvested 7 d.p.i. for analyses. **A)** Representative whole blot images from cytokine array performed on cardiac tissue lysate. **B)** Quantification of blots from cytokine array (n=4). Student's t-test. Data are represented as mean ± SEM.

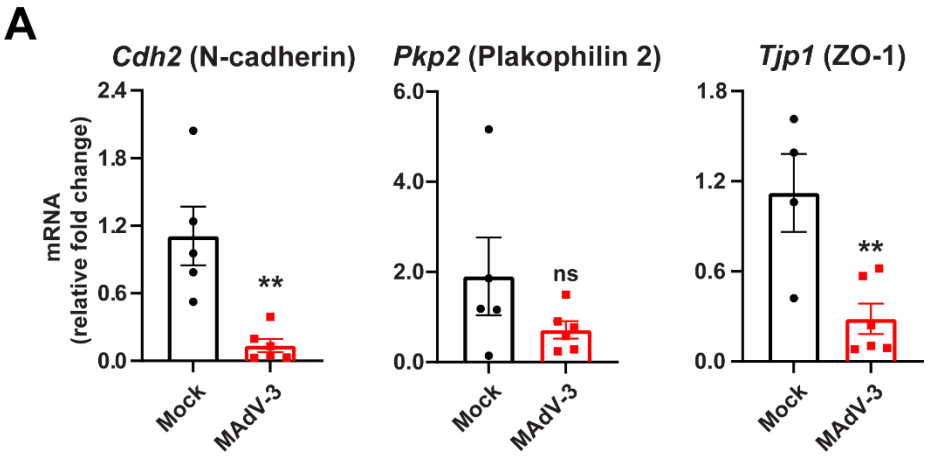

Supplemental Figure 3. Acute adenovirus infection alters intercalated disc junctional scaffolding gene expression. Mice were infected intranasally with $5x10^5$ i.u. MAdV-3 or saline (mock) and cardiac tissue was harvested 7 d.p.i. for analyses. **A)** RT-qPCR of heart tissue mRNA for major cardiac scaffolding genes *Cdh2*, *Pkp2*, and *Tjp1*, (n=5,6). **$p \leq 0.01$, student's t-test. Data are represented as mean ± SEM.

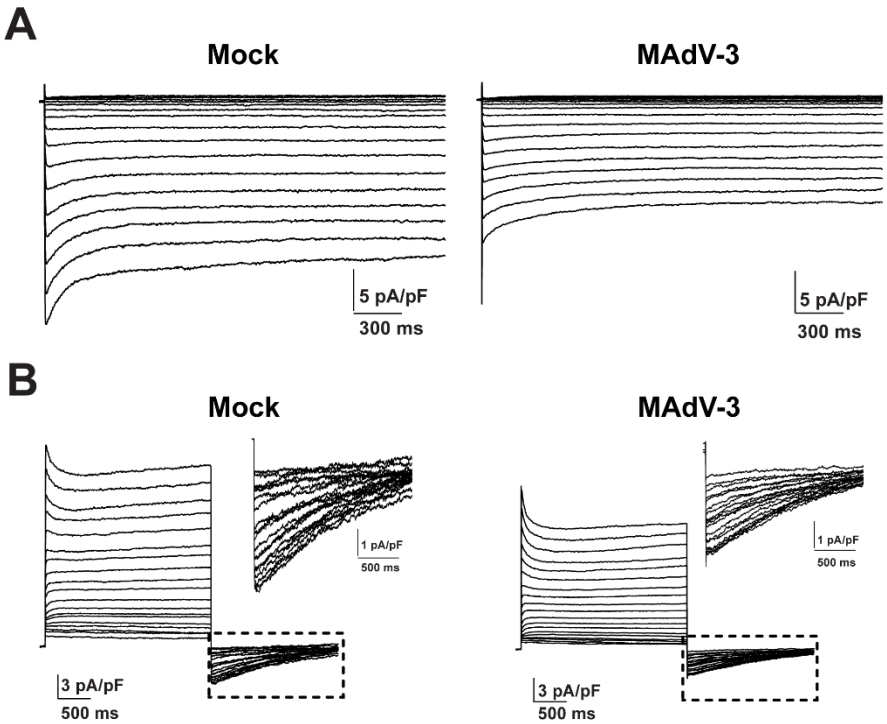

Supplemental Figure 4. Raw traces of I_{K1} and I_{Ks} currents. Isolated ACMs were infected with MAdV-3 at MOI 10 and were patch clamped at 24 h.p.i. **A)** Full current traces of I_{K1} in uninfected and infected cardiomyocytes. **B)** I_{Ks} insert currents measured in the presence of 5 μM E4031, n=19.